NASA TECHNICAL NOTE

NASA TN D-7650

AERODYNAMIC AND FLOW-VISUALIZATION STUDIES OF VARIATIONS IN THE GEOMETRY OF IRREGULAR PLANFORM WINGS AT A MACH NUMBER OF 20.3

by David R. Stone and Bernard Spencer, Jr.

Langley Research Center
Hampton, Va. 23665

1. Report No. NASA TN D-7650	2. Government Accession No.	3. Recipient's Catalog No.
4. Title and Subtitle AERODYNAMIC AND FLOW-VISUALIZATION STUDIES OF VARIATIONS IN THE GEOMETRY OF IRREGULAR PLANFORM WINGS AT A MACH NUMBER OF 20.3		5. Report Date August 1974
		6. Performing Organization Code
7. Author(s) David R. Stone and Bernard Spencer, Jr.		8. Performing Organization Report No. L-9382
9. Performing Organization Name and Address NASA Langley Research Center Hampton, Va. 23665		10. Work Unit No. 502-37-01-04
		11. Contract or Grant No.
12. Sponsoring Agency Name and Address National Aeronautics and Space Administration Washington, D.C. 20546		13. Type of Report and Period Covered Technical Note
		14. Sponsoring Agency Code

15. Supplementary Notes

16. Abstract

The longitudinal and summary lateral-directional stability characteristics have been obtained for a variety of irregular planform wings applied to a conceptual space shuttle orbiter. Three basic wing planforms with leading-edge sweep angles of 53.2^O, 46.8^O, and 35° were studied in conjunction with a series of inboard planform fillets with sweep angles up to 78°. The spanwise intersection point of the fillets and the basic wings was held constant. The data were obtained in the Langley 22-inch helium tunnel at a Mach number of 20.3 and a Reynolds number of 2.10×10^6 based on model length. Model angle-of-attack range was from 0° to 54° at sideslip angles of 0° and -3.8^O. Also included are results of a flow-visualization study consisting of electron-beam-illuminated flow and surface oil-flow patterns.

17. Key Words (Suggested by Author(s)) Space vehicles Hypersonic aerodynamics Flow visualization Irregular planform wings	18. Distribution Statement Unclassified — Unlimited STAR Category 31		
19. Security Classif. (of this report) Unclassified	20. Security Classif. (of this page) Unclassified	21. No. of Pages 56	22. Price* $3.75

AERODYNAMIC AND FLOW-VISUALIZATION STUDIES OF VARIATIONS

IN THE GEOMETRY OF IRREGULAR PLANFORM WINGS

AT A MACH NUMBER OF 20.3

By David R. Stone and Bernard Spencer, Jr.
Langley Research Center

SUMMARY

The longitudinal and summary lateral-directional stability characteristics have been obtained for a variety of irregular planform wings applied to a conceptual space shuttle orbiter. Three basic wing planforms with leading-edge sweep angles of 53.2^O, 46.8^O, and 35° were studied in conjunction with a series of inboard planform fillets with sweep angles up to 78°. The spanwise intersection point of the fillets and the basic wings was held constant. The data were obtained in the Langley 22-inch helium tunnel at a Mach number of 20.3 and a Reynolds number of 2.10×10^6 based on model length. Model angle-of-attack range was from 0° to 54° at sideslip angles of 0° and -3.8^O. Flow-visualization studies using both the surface oil-flow and electron-beam-illumination techniques were made for selected configurations and test conditions.

The results of the investigation indicate that the addition of fillets increased the maximum lift coefficient and trim angle of attack of the basic wings with negligible effect on longitudinal stability at trim. The addition of fillets had little effect on the static directional instability of the basic wing designs and slightly decreased the static lateral stability (positive effective dihedral); however, the dynamic directional stability parameter was favorable above an angle of attack of 14° for all wing-fillet combinations. The flow-visualization results indicated that the addition of the fillets had little effect on the location of the bow-shock—wing-shock interaction, which was inboard of the wing tips and outboard of the wing-fillet juncture at an angle of attack of 30°. The location of vortices and extent of vortex scrubbing on the side of the fuselage depended on the location of the body-fillet juncture.

INTRODUCTION

The NASA Langley Research Center has recently initiated an experimental and analytical program to study the aerodynamic characteristics of irregular planform wings (also referred to as cranked wings (ref. 1) or double delta wings (ref. 2)). For the present study, these planforms are referred to as wing-fillet combinations with the inboard

more highly swept portion of the planform being defined as a fillet according to the connotations of reference 3.

The study is at present directed toward improving the aerodynamics of the space shuttle orbiter, although the general long-range goals are applicable toward improved design of aircraft as well as certain advanced aerospace vehicles. The benefits to be derived from the use of fillets with selected planforms include linearization of the subsonic lift-curve slope to high angles of attack. (See ref. 4.) With regard to shuttle orbiter design, this improved lift at the angle of attack specified for landing allows for either reduced landing speeds or reduced wing planform area for specified mission return weight. In addition, proper tailoring of the wing-fillet combination allows linearization of the curve of pitch against the angle of attack up to angles for high lift; thus, trim penalties on both lift and performance are reduced. Although these subsonic benefits may be favorable, the question arises as to what effect a near-optimum subsonic design will have on the desired hypersonic trim angle and stability requirements (dictated by cross-range or heating constraints). Since both subsonic and hypersonic conditions are the two prime areas of concern in the present application of wing-fillet combinations, the overall study has been designated the Subsonic-Hypersonic Irregular Planforms Study (SHIPS).

With regard to the overall projected SHIPS program, the objectives of the study are to generate an experimental data base from low subsonic to hypersonic speeds accounting for secondary effects of Reynolds number, airfoil section, leading-edge radius and sweep, as well as planform geometry; to provide an aerodynamic prediction technique for irregular planform wings based on these extensive wind-tunnel results; and to provide empirically determined boundaries to serve as design guides regarding linearized lift, pitch, and realistic longitudinal and lateral center-of-pressure locations as a function of Mach number.

The present paper is an element of the SHIPS supporting information and presents the aerodynamic characteristics at a Mach number of 20.3 for a series of wing-fillet combinations on three wings which have each been separately studied on various orbiter concepts. The basic wings are designated: wing 1, a 53.2° clipped delta (refs. 5, 6, and 7); wing 2, a 46.8° trapezoidal design from an analytical program (ref. 8); and wing 3, a 35° trapezoidal design (ref. 9). A systematic series of fillet sweep angles up to 78° were examined with each wing while maintaining a constant spanwise intersection of the fillet and wing. The data were obtained at a Reynolds number of 2.10 $\times$ 10^6 based on model length over an angle-of-attack range of 0° to 54° at sideslip angles of 0° and approximately -3.8°. The basic aerodynamic data have been previously presented in reference 10.

The longitudinal force characteristics are referred to the stability axes, and the longitudinal moment and the lateral-directional characteristics are referred to the body axes. The coefficients are normalized with respect to the theoretical basic wing (that is, without fillet), planform area, body reference length, and total span of each wing. (See table I.) The characteristics of the body alone were normalized by using the reference dimensions of wing 1. The moment-reference point corresponds to a longitudinal center-of-gravity location at 0.66 body reference length and a vertical location on the body reference line. (See fig. 1.)

b wing span

C_A axial-force coefficient, $\dfrac{\text{Axial force}}{qS}$

C_D drag coefficient, $C_A \cos\alpha + C_N \sin\alpha$

C_L lift coefficient, $C_N \cos\alpha - C_A \sin\alpha$

C_l rolling-moment coefficient, $\dfrac{\text{Rolling moment}}{qSb}$

C_{l_β} rate of change of rolling-moment coefficient with sideslip angle, $\dfrac{\Delta C_l}{\Delta\beta}$, per degree ($\beta = 0^{\circ}$ and $\beta = -3.8^{\circ}$)

C_m pitching-moment coefficient, $\dfrac{\text{Pitching moment}}{qSl}$

C_N normal-force coefficient, $\dfrac{\text{Normal force}}{qS}$

C_n yawing-moment coefficient, $\dfrac{\text{Yawing moment}}{qSb}$

C_{n_β} rate of change of yawing-moment coefficient with sideslip angle, $\dfrac{\Delta C_n}{\Delta\beta}$, per degree ($\beta = 0^{\circ}$ and $\beta = -3.8^{\circ}$)

$\left(C_{n_\beta}\right)_{dyn}$ dynamic directional-stability parameter, $C_{n_\beta} \cos\alpha - C_{l_\beta} \dfrac{I_Z}{I_X} \sin\alpha$, per degree

C_Y side-force coefficient, $\dfrac{\text{Side force}}{qS}$

C_{Y_β} rate of change of side-force coefficient with sideslip angle, $\dfrac{\Delta C_Y}{\Delta\beta}$, per degree ($\beta = 0^{\circ}$ and $\beta = -3.8^{\circ}$)

I_Z/I_X ratio of moments of inertia about yaw and roll axes; value used = 7.0

L/D   lift-drag ratio

l body reference length

M   Mach number

q   dynamic pressure

S   reference planform area

S_f planform area of fillet

x   longitudinal coordinate measured from model nose

x_{cp} location of center of pressure measured from model nose

α angle of attack, deg

β sideslip angle, deg

Λ_f fillet leading-edge sweep angle, deg

Λ_w wing leading-edge sweep angle, deg

Subscripts:

max   maximum

trim   trim conditions, $C_m = 0$

MODELS

The fuselage for the present investigation was a 0.00403-scale version of the LO-100 orbiter concept (ref. 5). The fuselage forebody incorporated positive camber to produce near zero or positive pitching moment at zero angle of attack at hypersonic speeds. A body base flap was also included as a hypersonic trim device.

Wing 1 (fig. 1(a)) had a 53.2° leading-edge sweep, unswept trailing edge, 1° of incidence at the theoretical root, and -4° incidence at the tip. Wing 2 (fig. 1(b)) had a 46.8° leading-edge sweep, -11.2° trailing-edge sweep, and a 1.5° incidence. Wing 3 (fig. 1(c)) had a 35° leading-edge sweep, -19.6° trailing-edge sweep, and a 1.5° incidence. A more detailed description of the model components is listed in table I.

The longitudinal location of each wing on the fuselage was selected to produce a wing-fillet intersection at 0.62 of the body reference length with a spanwise intersection at 0.176 (normalized by the body reference length). Fillet sweeps to 78° (table II) were investigated on each wing while a constant spanwise intersection of the fillet and wings was maintained. Fillet leading-edge radius was dictated by the minimum allowable from aerodynamic heating constraints for a given fillet sweep (that is, reduced sweep and increasing radii). No specific airfoil section applies to the fillets and maximum thickness occurs where each fillet fairs into the basic wing along the wing maximum thickness line (that is, line at constant percent of chord).

APPARATUS AND TESTS

Wind Tunnel

The experimental investigation was conducted in the Langley 22-inch helium tunnel at a Mach number of 20.3 and a Reynolds number of 2.1×10^6 based on model length (13.823 cm). The total temperature of the flow was within the range of about 278 to 288 K. Operational characteristics of the facility and details of the contoured nozzle flow calibrations are available in reference 11.

Tests

Aerodynamic characteristics.- The various configurations were tested on sting-supported six-component strain-gage balances. Two balance-sting combinations were used to cover the angle-of-attack range of 0° to 54°: a straight sting for $0° \leqq \alpha \leqq 35°$ and a 35° bent sting for $18° \leqq \alpha \leqq 54°$. A detailed description of the stings is given in reference 12. Data were obtained at predetermined angles of attack by using a prism mounted in the model to reflect light from a point (adjacent to the test-section window) onto electric eyes positioned at calibrated intervals. Additional features of this system can be found in reference 11. Sideslip angles were obtained with the sting yawed at fixed angles of 0° and approximately -3.8°.

The estimated maximum uncertainties in the measured basic data and in the test conditions are shown in the following table:

	Straight sting	35° bent sting
C_N	±0.0047	±0.0142
C_A	±0.0016	±0.0020
C_m	±0.0012	±0.0021
C_l	±0.0004	
C_n	±0.0004	
C_Y	±0.0032	
α, β, deg	±0.1	
$\dot{M}$	±0.2	

Uncertainties in the aerodynamic coefficients and the test parameters were determined from a static calibration of the balance, readout errors, and test-section Mach number calibrations. Base pressures were measured at one location for the low-angle-of-attack tests, and the balance axial forces were adjusted to a condition in which free-stream pressure acted over the model base. Since these corrections at higher angles of attack are negligible (ref. 12), the data for the high-angle-of-attack tests contain no base pressure corrections.

Flow visualization.- Both surface oil-flow and electron-beam illumination techniques were employed to study the flow characteristics. The technique used for the surface oil-flow studies was to apply droplets of a mixture of lampblack and silicone oil onto a light-colored model that had been initially coated with a thin film of clear silicone oil. Simultaneous photographs of the oil-flow patterns and the electron-beam illuminated flow field were then made during a run. Additional photographs of the oil-flow patterns were taken after the models were removed from the tunnel. Although a model shield device was used, these patterns were subjected to flow shutdown disturbances. These disturbances have been observed to be small, but they can cause a slight movement in heavy oil accumulation regions such as along separation lines.

The electron beam is routinely used as a flow-visualization device in the 22-inch helium tunnel. The flow becomes illuminated when the gas molecules radiate light upon returning from a momentarily excited state caused by a bombardment of electrons from a concentrated beam emitted from a gun device. The light-intensity variations, proportional to the gas density, permit flexible, three-dimensional viewing of the external flow field about a test model. More details of the equipment and a description of the illuminated flow technique can be found in reference 13.

RESULTS AND DISCUSSION

Aerodynamic Characteristics

The longitudinal aerodynamic characteristics of the body alone and each of the wing-body combinations (without fillets) are presented in figure 2. The lift coefficient increased

with decreasing wing leading-edge sweep; however, the $(L/D)_{max}$ decreased with decreasing wing leading-edge sweep (from 2.05 for wing 1 to 1.75 for wing 3) because of higher wave drag for lower sweep angles. As expected, the body alone was longitudinally unstable over the test angle-of-attack range for the selected center-of-gravity location of 0.66 body length. All three wing-body combinations were longitudinally stable for angles of attack from 14° to 51°, and trim occurred at $\alpha = 17^O$ (wing 1), $\alpha = 18^O$ (wing 3), and $\alpha = 20^O$ (wing 2).

The longitudinal characteristics of the three wing-body combinations with fillets are given in figures 3, 4, and 5 and are summarized in figure 6. The addition of the fillets increased the $C_{L,max}$ (fig. 6(a)) of each basic wing whereas α for $C_{L,max}$ remained unchanged ($\alpha = 51^O$). The increase in $C_{L,max}$ for the largest fillet $\left(\Lambda_f = 78^O\right)$ was 0.03 for wing 1, 0.045 for wing 2, and 0.055 for wing 3. The value of $(L/D)_{max}$ increased slightly with wing fillet sweep (approximately 0.10 for the largest fillet on each basic wing). Increasing wing fillet sweep for any given wing increased α_{trim} with stable trim points being obtained. Analysis of the pitch data indicated that the addition of fillets on each wing design had negligible effect on longitudinal stability at trim with some loss in longitudinal stability above α_{trim}. The increase in α_{trim} (fig. 6(b)) for both wing 2 and wing 3 was slightly greater than 10°, which was sufficient to trim the vehicle near $\alpha = 30^O$ (nominal entry attitude for a shuttle orbiter high-cross-range mission, ref. 14) with neutral elevon control.

The summary lateral-directional characteristics for each of the wing-body combinations (without fillets) are presented in figure 7. All three wings had relatively constant levels of static directional instability $\left(-C_{n_\beta}\right)$ except for wing 3 above $\alpha = 20^O$ and positive effective dihedral $\left(-C_{l_\beta}\right)$ which increased with increasing angle of attack. The dynamic directional stability parameter $\left(\left(C_{n_\beta}\right)_{dyn}\right)$ was positive (favorable) above $\alpha = 14^O$. The addition of the 70° and 78° fillets on wing 2 (fig. 8) had a small effect on the static directional instability and slightly decreased the positive effective dihedral above $\alpha = 20^O$.

Flow-Visualization Studies

Flow-visualization studies were conducted to observe the flow about the orbiter with various wing fillets in order to identify any complex flow phenomena due to the complicated geometry. Electron-beam and oil-flow photographs using combinations of basic wing 2 (fillet off) and with 65° and 78° fillets at angles of attack of 30° and 40° are presented in figures 9 to 20. Electron-beam photographs of the other wings at $\alpha = 30^O$ are presented in figures 21 and 22.

The illuminated-flow results for wing 2 indicate that the location of the interaction between the bow and wing shocks was relatively unchanged by the addition of fillets and was located substantially inboard of the wing tips but outboard of the wing-fillet juncture

at $\alpha = 30^{\circ}$ (figs. 9(b), 9(c), 10(b), 10(c), and 11(b)). The interaction was near the wing tips at $\alpha = 40^{\circ}$ (figs. 12(b), 12(c), 13(b), 13(c), and 14(b)). Under flight conditions, the shocks would be more inboard since shock-detachment distances are generally smaller in air because of its lower ratio of specific heats compared with the helium test medium.

The oil-flow patterns (figs. 15 to 20) show extensive attached flow along the side of the fuselage forward of the fillet, vortex-type flow from the fillet-body junctures that sweep the side of the body, and substantial attached flow along the upper surfaces of the wing at $\alpha = 30^{\circ}$. Note that in figure 10 some rearward movement of the oil along the separation lines of the upper surface of the wing occurred after shutdown. The location of vortices and extent of scrubbing on the side of the fuselage depends on the location of the fillet-body juncture. (See figs. 15(c), 16(c), and 17(c).) It should be noted that this type of vortex scrubbing also occurs for other delta-wing configurations. (See, for example, ref. 12.) In the bottom views there was extensive outflow along the forebody of the fuselage and fillets, inflow near the wing-fillet junctures, and outflow on the wing outboard of the bow and wing-shock interaction; however, the flow on the bottom of the wing in the area of the undeflected elevon controls and body flap was essentially two-dimensional. (See (b) parts of figs. 15 to 20.)

Electron-beam photographs showing the effect of the fillets on the shock structure of the body plus wings 1 and 3 at $\alpha = 30^{\circ}$ are given in figures 21 and 22, respectively. The addition of the fillets had little effect on the location of the interaction between the bow and wing shocks (as was the case for wing 2). Note that the 70° fillet angle generates an additional internal shock (figs. 21(b) and 22(b)) which interacts with the external shock structure. A similar internal shock can be seen for the 65° fillet-wing 2 combination in figure 10(c). This shock further complicates the flow field and could cause increased heating especially along the leading edge of the wing. A different fairing of the fillet body juncture (eliminating the break) could alleviate the generation of the undesirable internal shock.

CONCLUSIONS

The longitudinal and summary lateral-directional stability characteristics have been obtained in the Langley 22-inch helium tunnel for a variety of wing planforms having leading-edge sweep angles of 53.2°, 46.8°, and 35° in conjunction with a series of inboard planform fillets with sweep angles up to 78°. The spanwise intersection point of the fillets and the basic wings was held constant. A flow-visualization study consisting of electron-beam illuminated flow and surface oil-flow patterns was also included. The results of the investigation are as follows:

8

1. The addition of fillets increased the maximum lift coefficient and trim angle of attack of the basic wings with negligible effect on longitudinal stability at trim.

2. The addition of fillets had little effect on the static directional instability of the basic wing designs and slightly decreased the static lateral stability (positive effective dihedral); however, the dynamic directional stability parameter was favorable above an angle of attack of 14° for all wing-fillet combinations.

3. The flow-visualization results indicated that the addition of the fillets had little effect on the location of the bow-shock—wing-shock interaction, which was inboard of the wing tips and outboard of the wing-fillet juncture at an angle of attack of 30°. The location of vortices and extent of vortex scrubbing on the side of the fuselage depended on the location of the body-fillet juncture.

Langley Research Center,
  National Aeronautics and Space Administration,
    Hampton, Va., April 17, 1974.

REFERENCES

1. Hopkins, Edward J.; Hicks, Raymond M.; and Carmichael, Ralph L.: Effects of Planform Variations on the Aerodynamic Characteristics of Low-Aspect-Ratio Wing With Cranked Leading Edges. Conference on Aircraft Aerodynamics, NASA SP-124, 1966, pp. 469-483.

2. Corsiglia, Victor R.; Koenig, David G.; and Morelli, Joseph P.: Large-Scale Tests of an Airplane Model With a Double Delta Wing, Including Longitudinal and Lateral Characteristics and Ground Effects. NASA TN D-5102, 1969.

3. Love, Eugene S.: Advanced Technology and the Space Shuttle. Astronaut. & Aeronaut., vol. 11, no. 2, Feb. 1973, pp. 30-66.

4. Ray, Edward J.; McKinney, Linwood W.; and Carmichael, Julian G.: Maneuver and Buffet Characteristics of Fighter Aircraft. NASA TN D-7131, 1973.

5. Stone, David R.: Static Aerodynamic Characteristics and Oil Flow and Electron Beam Illumination Results of a 0.005 Scale Model Langley Concept Space Shuttle Orbiter (LO-100) at a Mach Number of 20.3. DMS-DR-2023 (Contract No. NAS 9-13247), Chrysler Corp. Space Div., May 1973. (Available as NASA CR-128763.)

6. Bernot, Peter T.: Hypersonic Performance, Stability and Control Characteristics of a 0.010 Scale Model of a Langley Concept Space Shuttle Orbiter (LO-100). DMS-DR-2031 (Contract No. NAS 9-13247), Chrysler Corp. Space Div., June 1973. (Available as NASA CR-128769.)

7. Spencer, Bernard, Jr.; and Fournier, Roger H.: Supersonic Stability and Control Characteristics of a Langley Concept Space Shuttle Orbiter (LO-100) at Mach Numbers of 1.5 to 4.63. DMS-DR-2033 (Contract No. NAS 9-13247), Chrysler Corp. Space Div., July 1973. (Available as NASA CR-128772.)

8. Phillips, W. Pelham; Decker, John P.; Rau, Timothy R.; and Glatt, C. R.: Computer-Aided Space Shuttle Orbiter Wing Design Study. NASA TN D-7478, 1974.

9. Spencer, Bernard, Jr.; and Ware, George M.: Low Subsonic Aerodynamic Characteristics of a Shuttle Orbiter Having 35° Trapezoidal Wing and 75° Inboard Glove. NASA TM X-2701, 1973.

10. Stone, David R.; and Spencer, Bernard, Jr.: Aerodynamic and Flow-Visualization Studies Associated With Variations in the Geometry of the Forward Portion of Irregular Planform Wings at a Mach Number of 20.3. DMS-DR-2036 (Contract No. NAS 9-13247), Chrysler Corp. Space Div., July 1973. (Available as NASA CR-128755.)

11. Arrington, James P.; Joiner, Roy C., Jr.; and Henderson, Arthur, Jr.: Longitudinal Characteristics of Several Configurations at Hypersonic Mach Numbers in Conical and Contoured Nozzles. NASA TN D-2489, 1964.

12. Arrington, James P.; and Stone, David R.: Aerodynamic and Flow-Visualization Studies of Two Delta-Wing Entry Vehicles at a Mach Number of 20.3. NASA TN D-7282, 1973.

13. Weinstein, Leonard M.; Wagner, Richard D., Jr.; Henderson, Arthur, Jr.; and Ocheltree, Stewart L.: Electron Beam Flow Visualization in Hypersonic Helium Flow. Paper presented at the 1969 IEEE Third International Congress on Instrumentation in Aerospace Simulation Facilities (Farmingdale, N.Y.), May 1969.

14. Ware, George M.; Spencer, Bernard, Jr.; and Fournier, Roger H.: Supersonic Aerodynamic Characteristics of the North American Rockwell ATP Shuttle Orbiter. NASA TM X-2804, 1973.

TABLE I.- GEOMETRIC CHARACTERISTICS OF THE MODEL

Body:
Reference length,[a] cm (in.) 13.823 (5.442)
Maximum height, cm (in.) 2.365 (0.931)
Maximum width, cm (in.) 2.580 (1.016)

Wing 1:
Root chord, cm (in.) 8.462 (3.332)
Tip chord, cm (in.) 1.269 (0.500)
Mean aerodynamic chord, cm (in.) 5.752 (2.265)
Span,[a] cm (in.) 10.762 (4.238)
Total planform area,[a] cm² (in²) 52.377 (8.118)
Leading-edge sweep, deg 53.2
Trailing-edge sweep, deg 0.0
Dihedral, deg 7.0
Incidence, deg . . . . 1° at root, -4° at tip
Airfoil section . . . . {NACA 0006-64 inboard / NACA 0012-64 tip
Aspect ratio 2.212
Taper ratio 0.15

Wing 2:
Root chord, cm (in.) 8.107 (3.192)
Tip chord, cm (in.) 1.092 (0.430)
Mean aerodynamic chord, cm (in.) 5.491 (2.162)
Span,[a] cm (in.) 11.114 (4.376)
Total planform area,[a] cm² (in²) 51.097 (7.920)
Leading-edge sweep, deg 46.8
Trailing-edge sweep, deg . . . . -11.2
Dihedral, deg 7.0
Incidence, deg 1.5
Airfoil section . . . . {NACA 0008-64 inboard / NACA 0012-64 tip
Aspect ratio 2.415
Taper ratio 0.135

Wing 3:
Root chord, cm (in.) 7.534 (2.966)
Tip chord, cm (in.) 1.506 (0.593)
Mean aerodynamic chord, cm (in.) 5.190 (2.043)
Span,[a] cm (in.) 11.414 (4.494)
Total planform area,[a] cm² (in²) 51.600 (7.998)
Leading-edge sweep, deg 35.0
Trailing-edge sweep, deg . . . . -19.6
Dihedral, deg 7.0
Incidence, deg 1.5
Airfoil section . . . . NACA 0008-64
Aspect ratio 2.525
Taper ratio 0.20

Vertical tail:
Root chord (exposed), cm (in.) 2.948 (1.160)
Tip chord, cm (in.) 1.216 (0.479)
Span (exposed), cm (in.) 2.943 (1.159)
Area (exposed), cm² (in²) 6.127 (0.950)
Leading-edge sweep, deg 45.0
Trailing-edge sweep, deg 25.0
Airfoil section . . . . NACA 0012-64
Aspect ratio 1.414
Taper ratio 0.412

Body flap:
Span, cm (in.) 2.355 (0.927)
Chord, cm (in.) 0.815 (0.321)
Area, cm² (in²) 0.960 (0.149)

[a] Model reference dimensions.

TABLE II.- PLANFORM AREA OF FILLETS

Λ_f, deg	S_f/S
Wing 1	
78	0.382
75	.272
70	.161
60	.046
Wing 2	
78	0.421
75	.309
70	.195
60	.078
Wing 3	
78	0.459
75	.348
70	.235
60	.119
50	.057
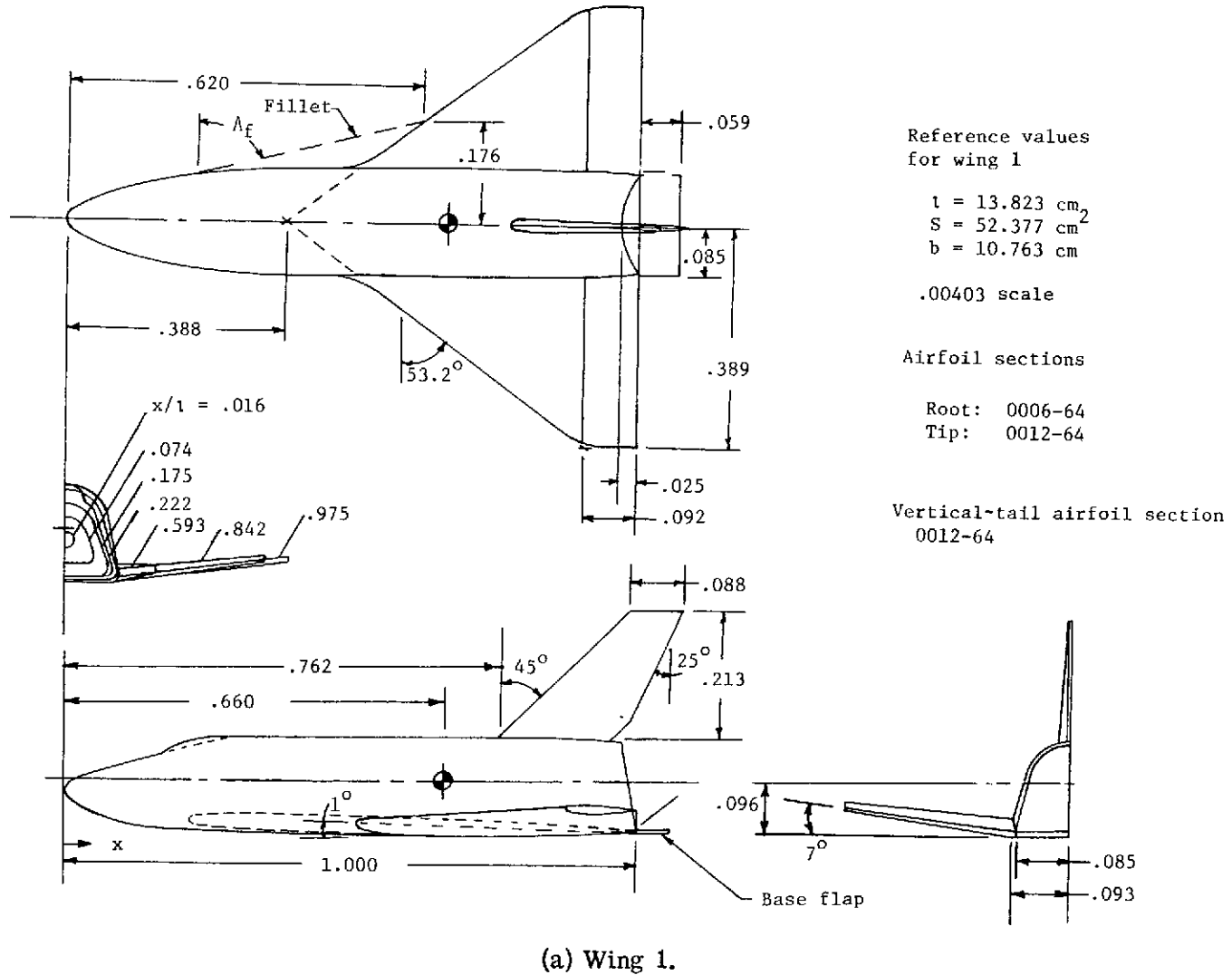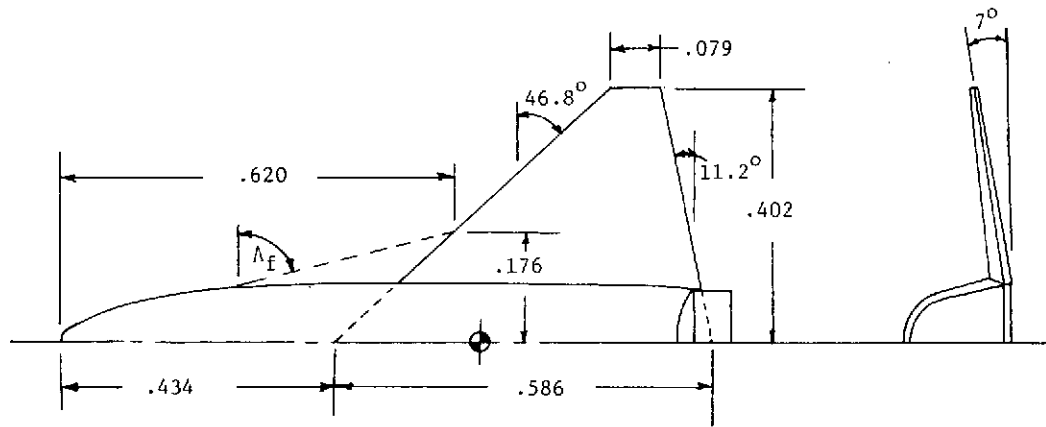
Reference values
for wing 1

l = 13.823 cm
S = 52.377 cm^2
b = 10.763 cm

.00403 scale

Airfoil sections

Root: 0006-64
Tip: 0012-64

Vertical-tail airfoil section
0012-64

(a) Wing 1.

Figure 1.- Sketch of models with dimensions normalized by body length l (13.823 cm).

(b) Wing 2.

(c) Wing 3.

Figure 1.- Concluded.
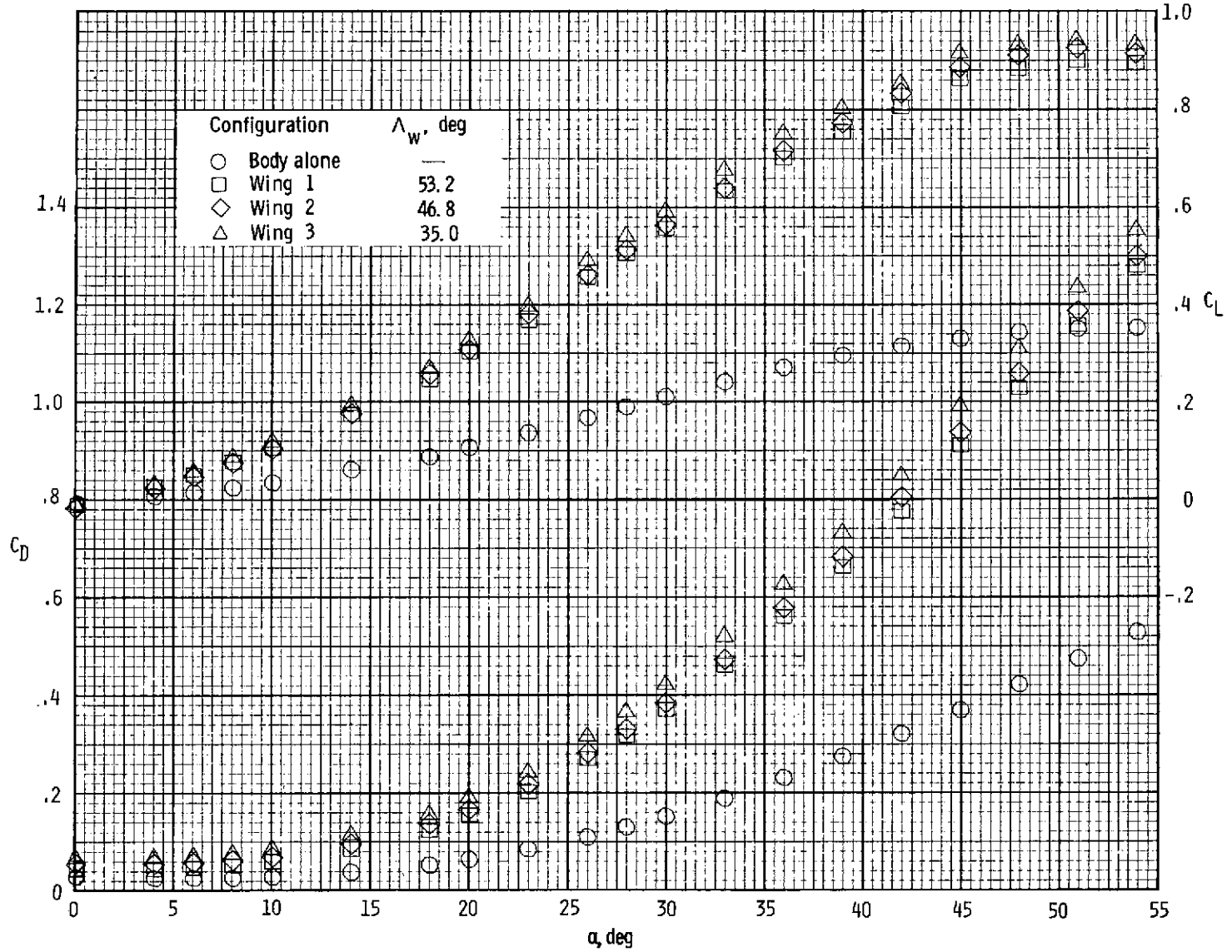
Figure 2.- Effect on longitudinal characteristics of adding the three wings (without fillets) to the fuselage.
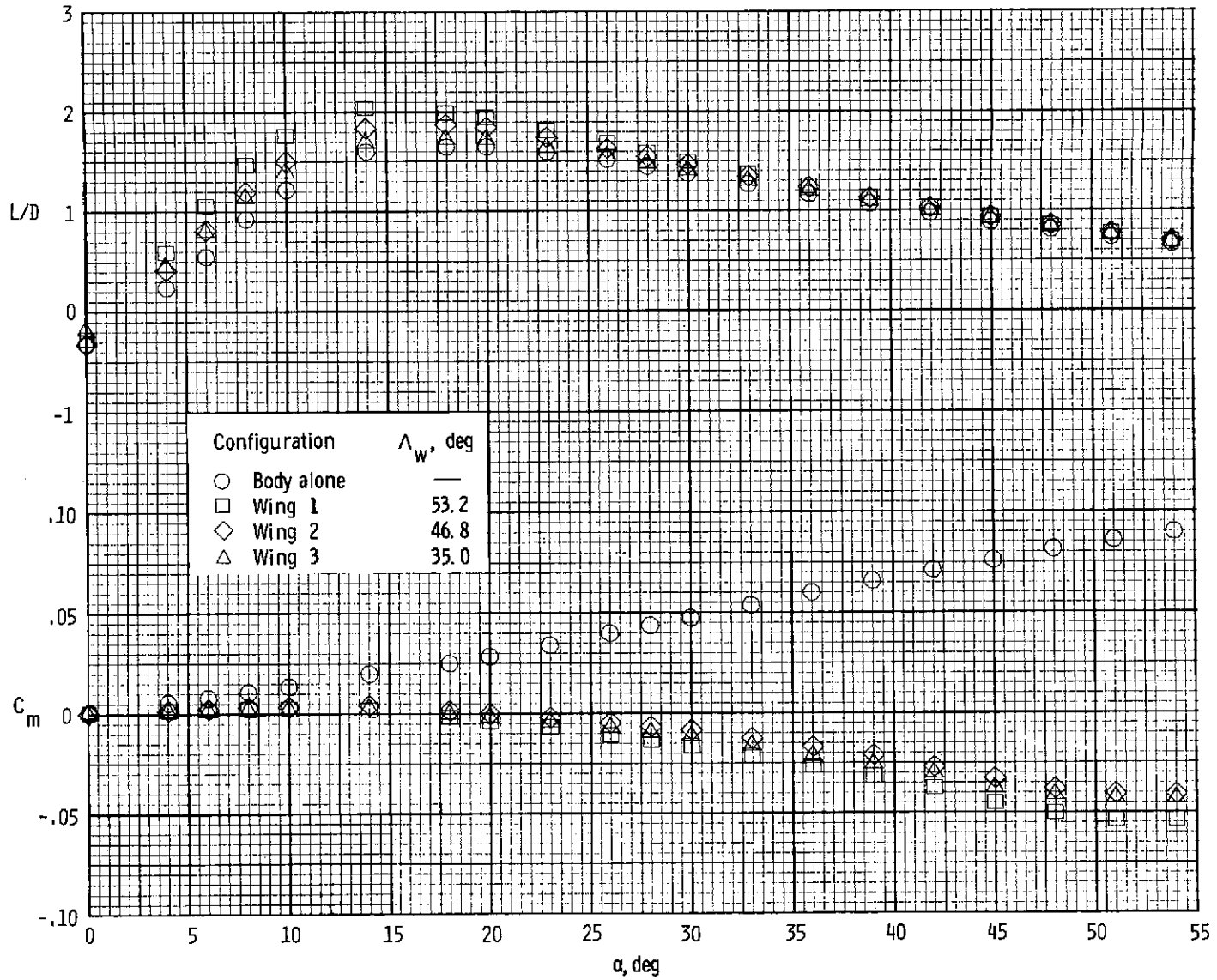
Figure 2.- Concluded.
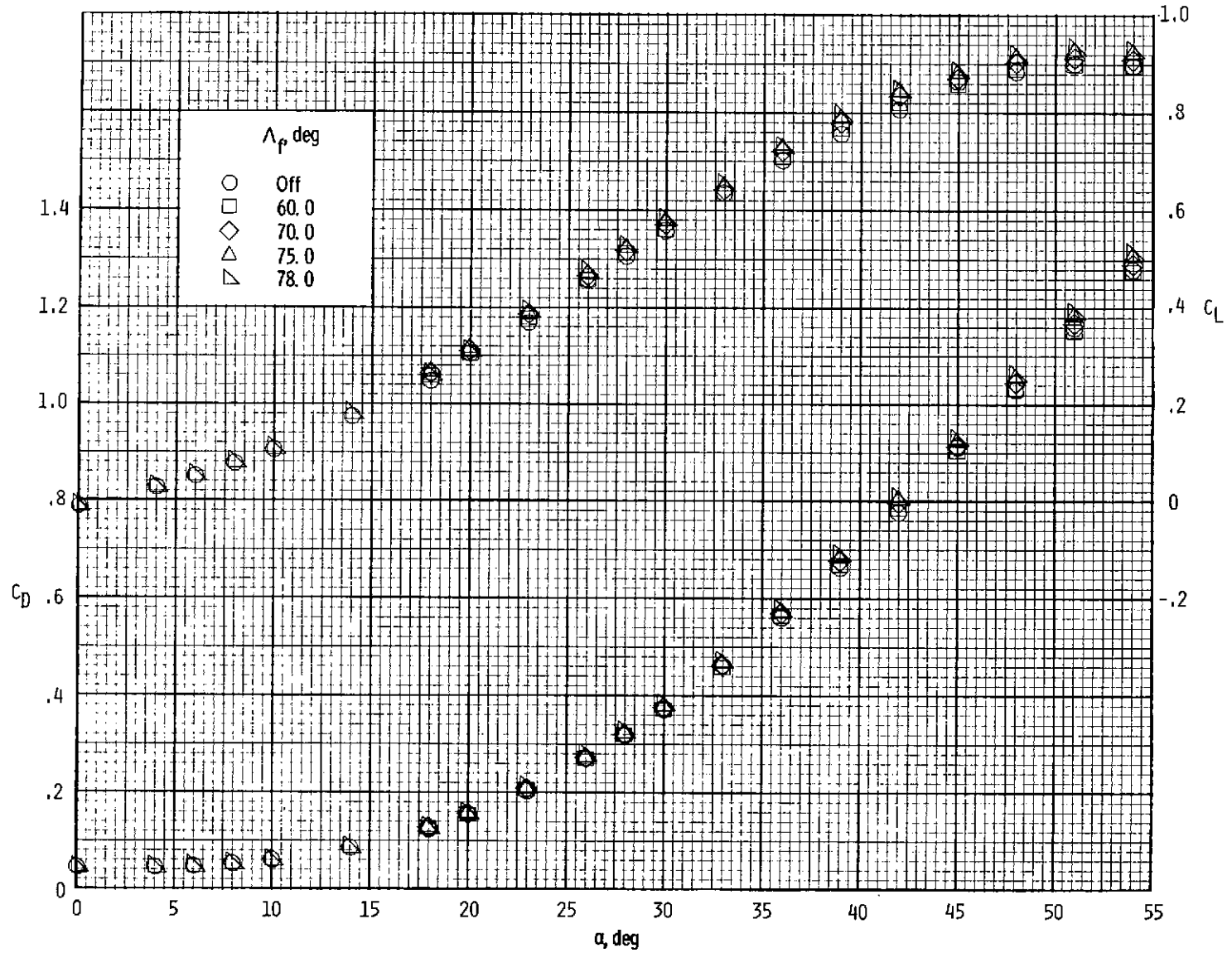
Figure 3.- Effect of fillets on the longitudinal characteristics of the body plus wing 1. $\Lambda_{\mathrm{w}} = 53.2^{\mathrm{O}}$.
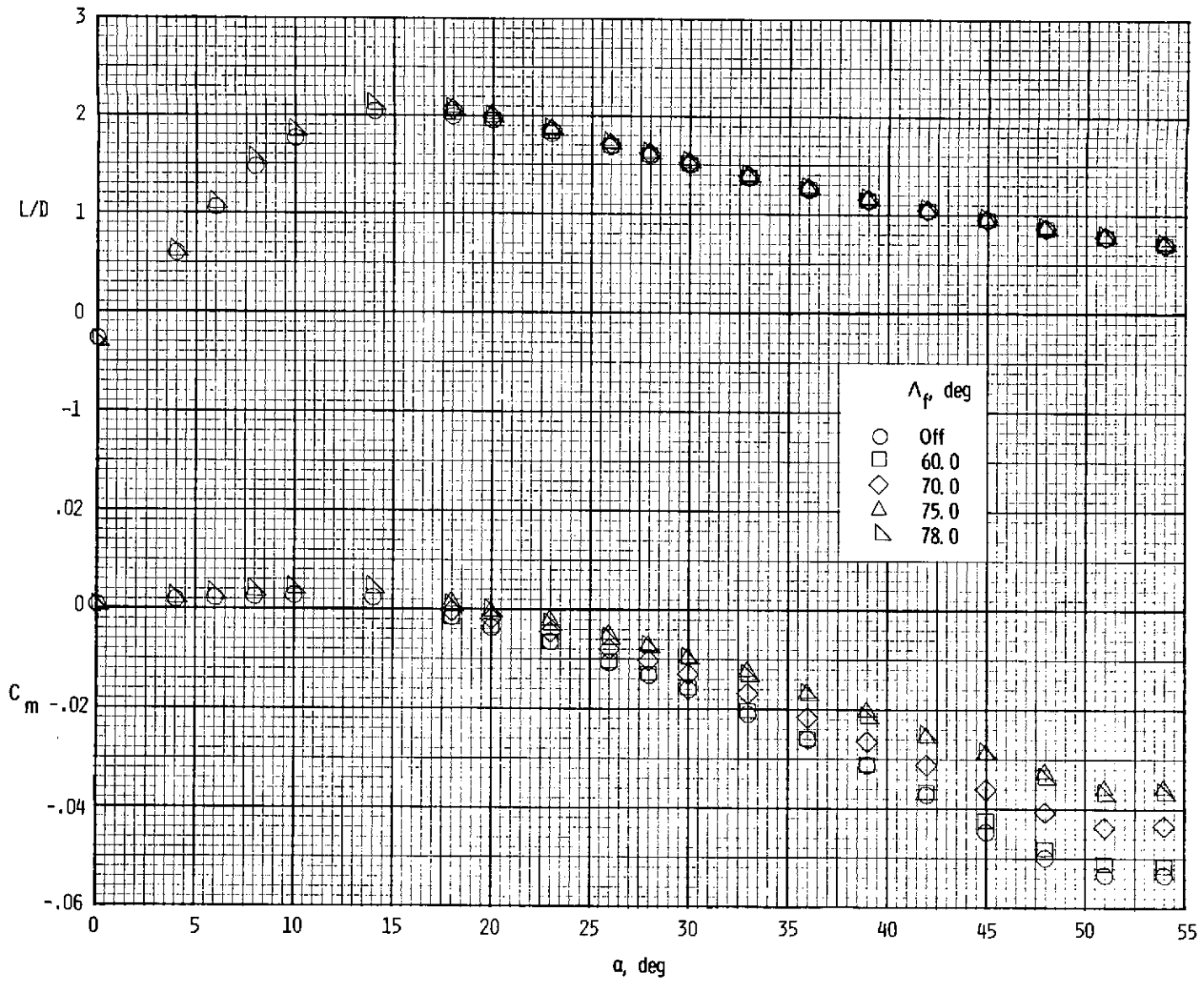
Figure 3.- Concluded.
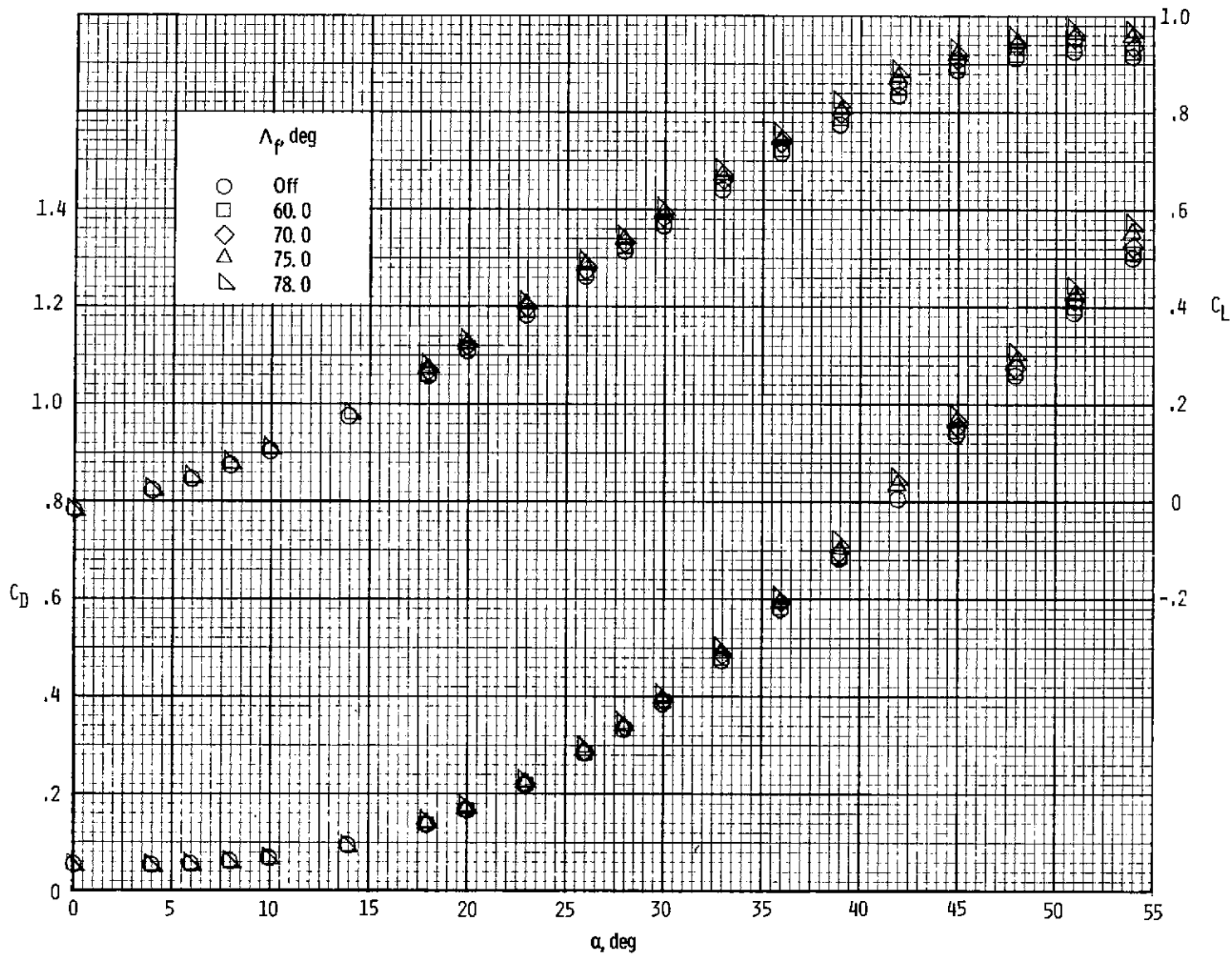
Figure 4.- Effect of fillets on the longitudinal characteristics of the body plus wing 2. $\Lambda_w = 46.8^o$.
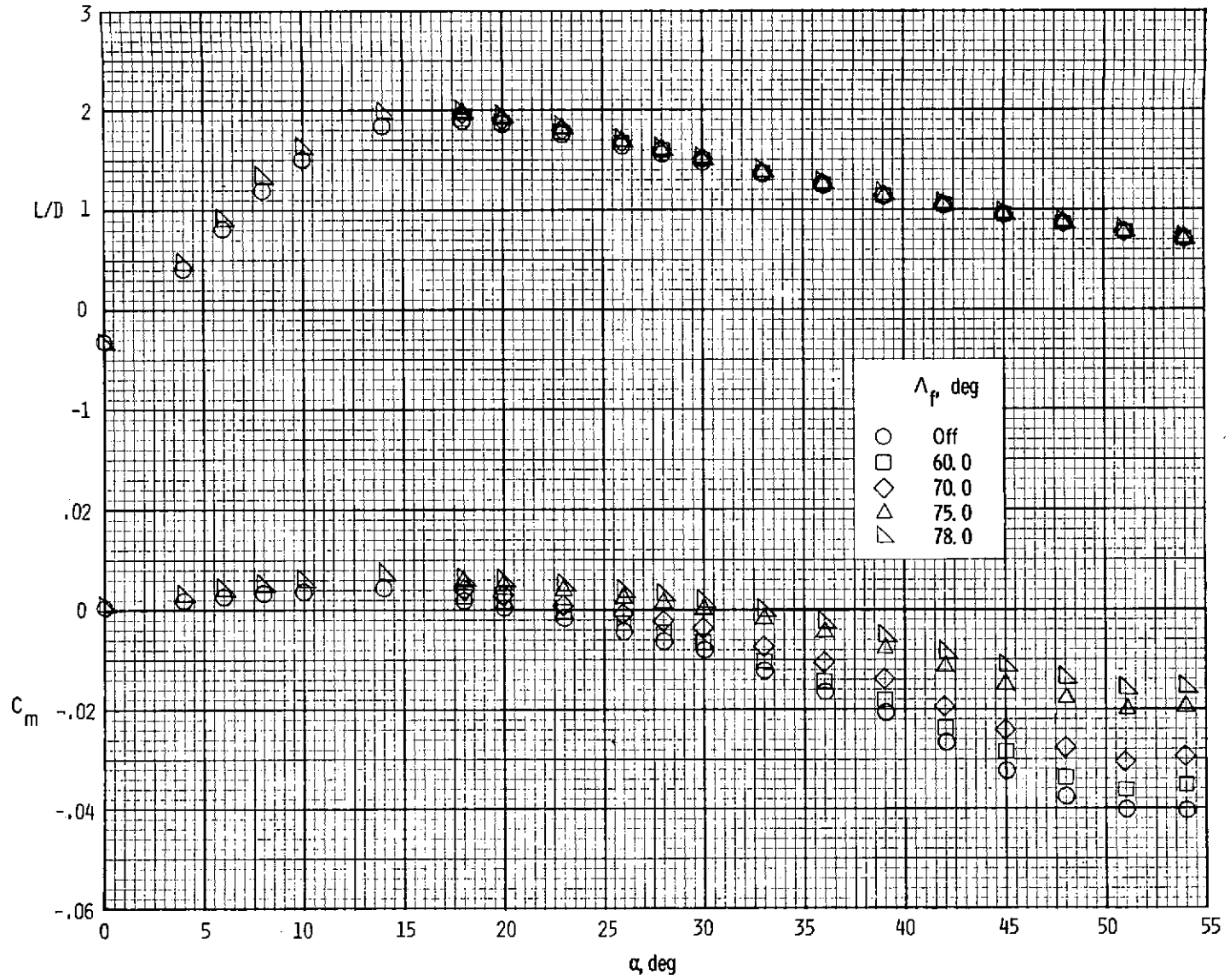
Figure 4.- Concluded.
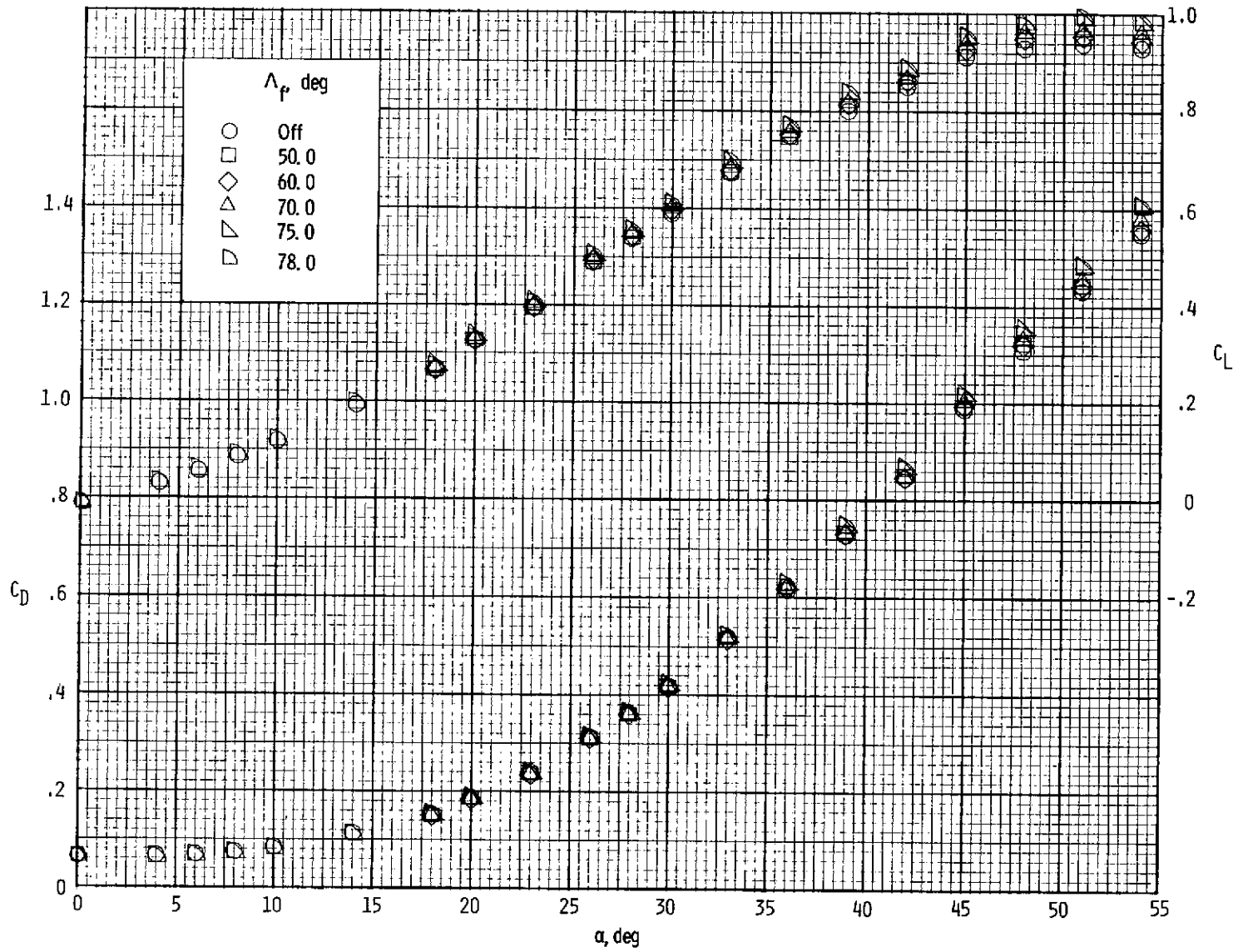
Figure 5.- Effect of fillets on the longitudinal characteristics of the body plus wing 3. $\Lambda_w = 35^o$.
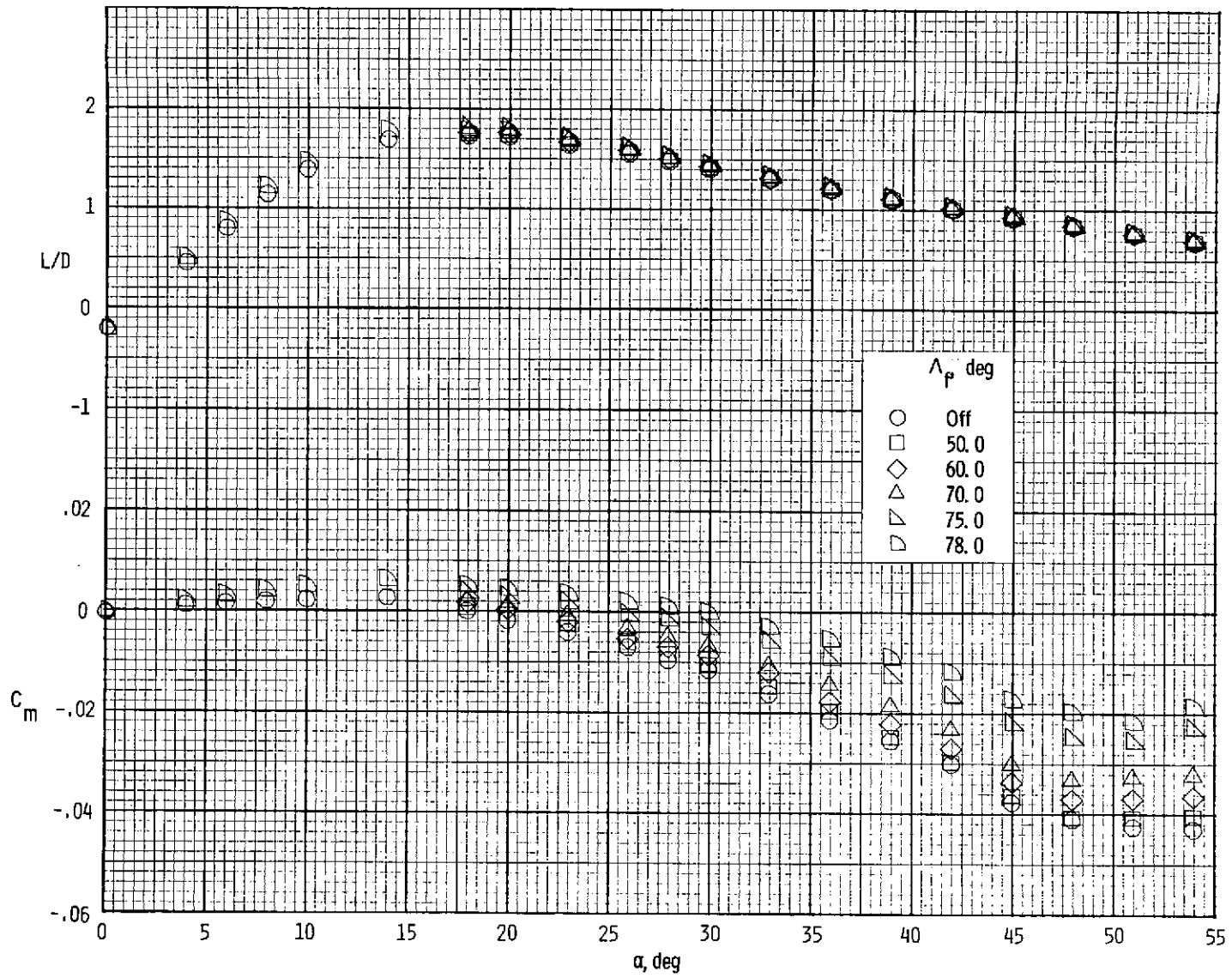
Figure 5.- Concluded.
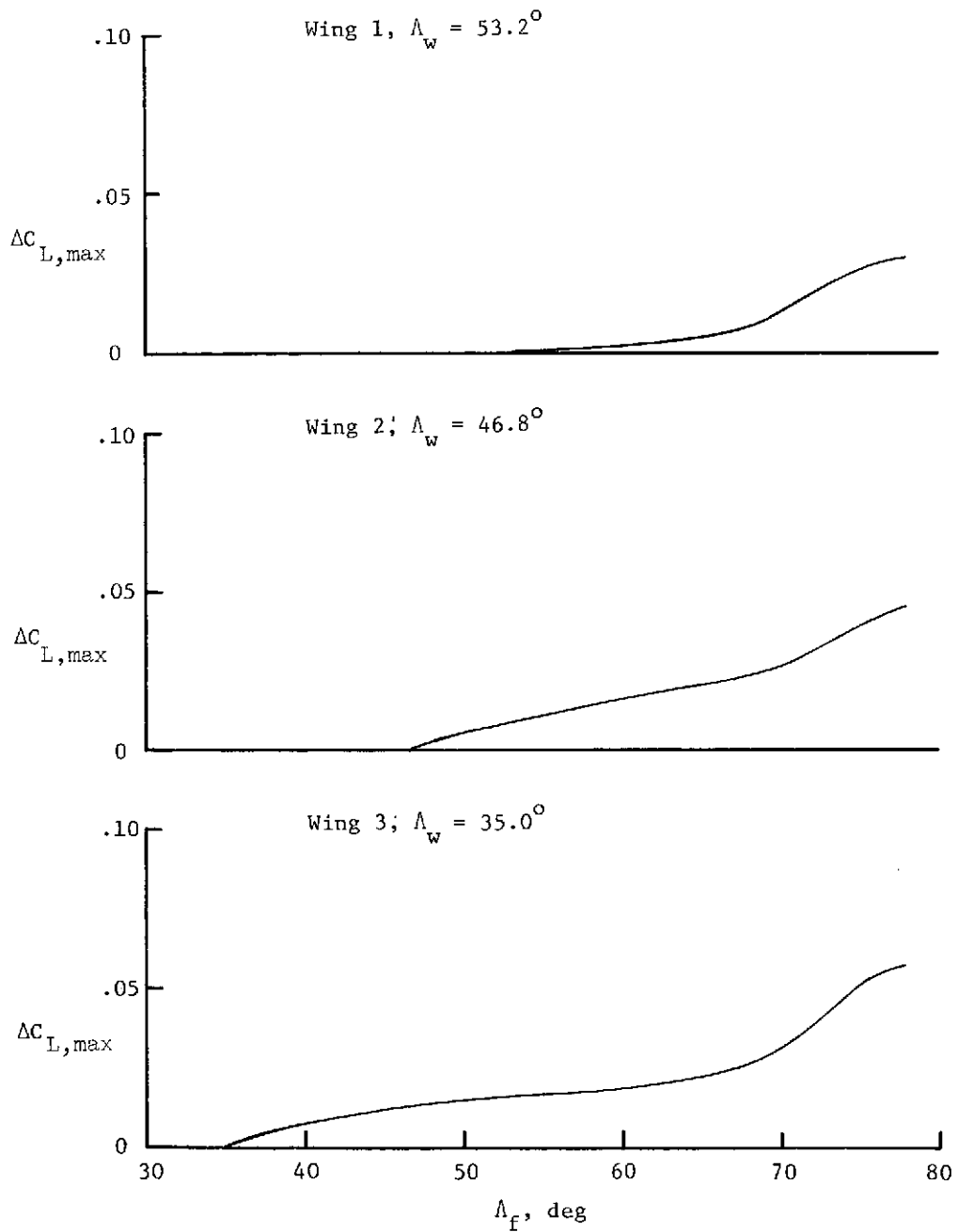
(a) Maximum lift coefficient.

Figure 6.- Effect of fillet sweep angle on summary longitudinal aerodynamics.
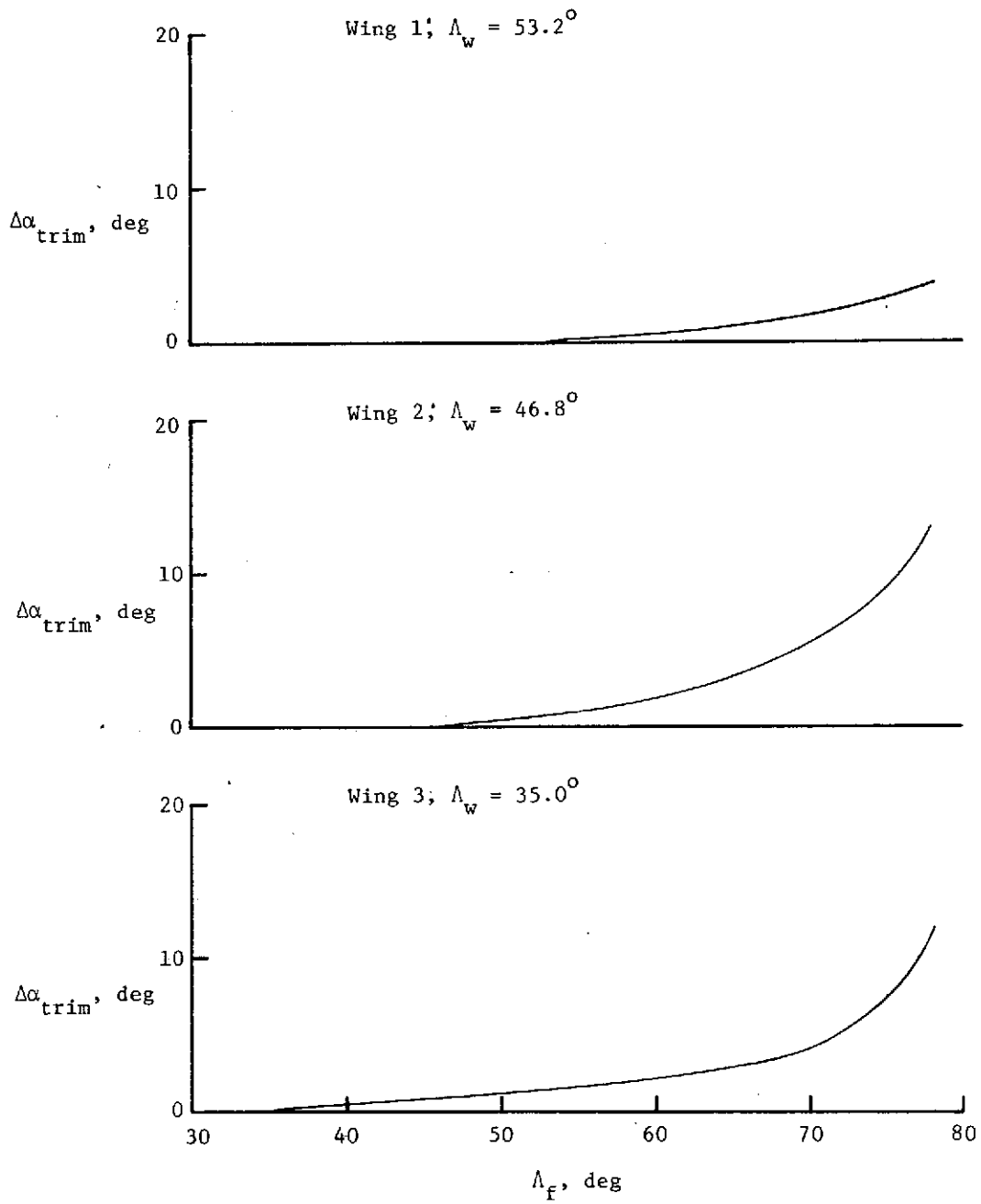
(b) Trim angle of attack.

Figure 6.- Continued.
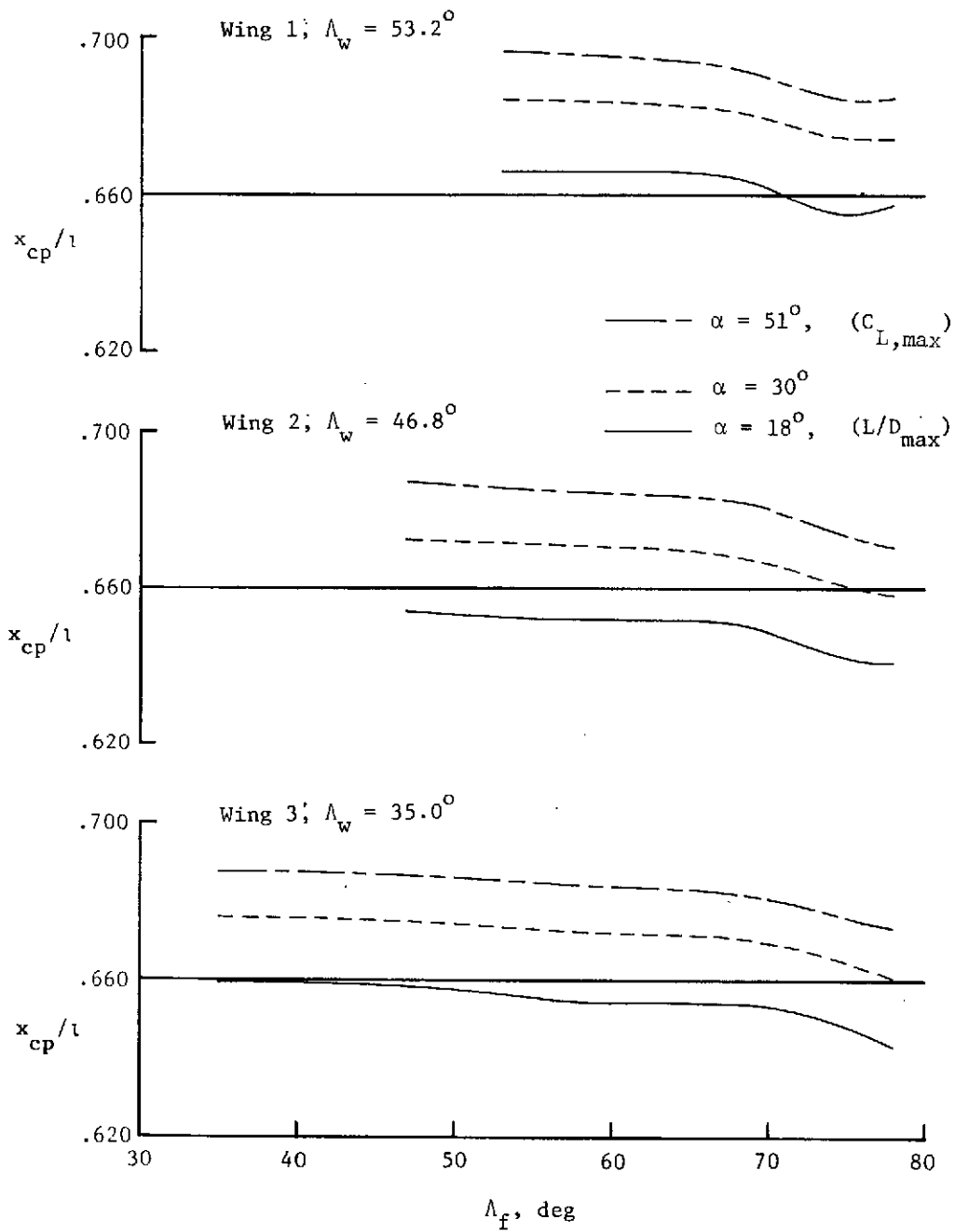
(c) Center of pressure.

Figure 6.- Concluded.
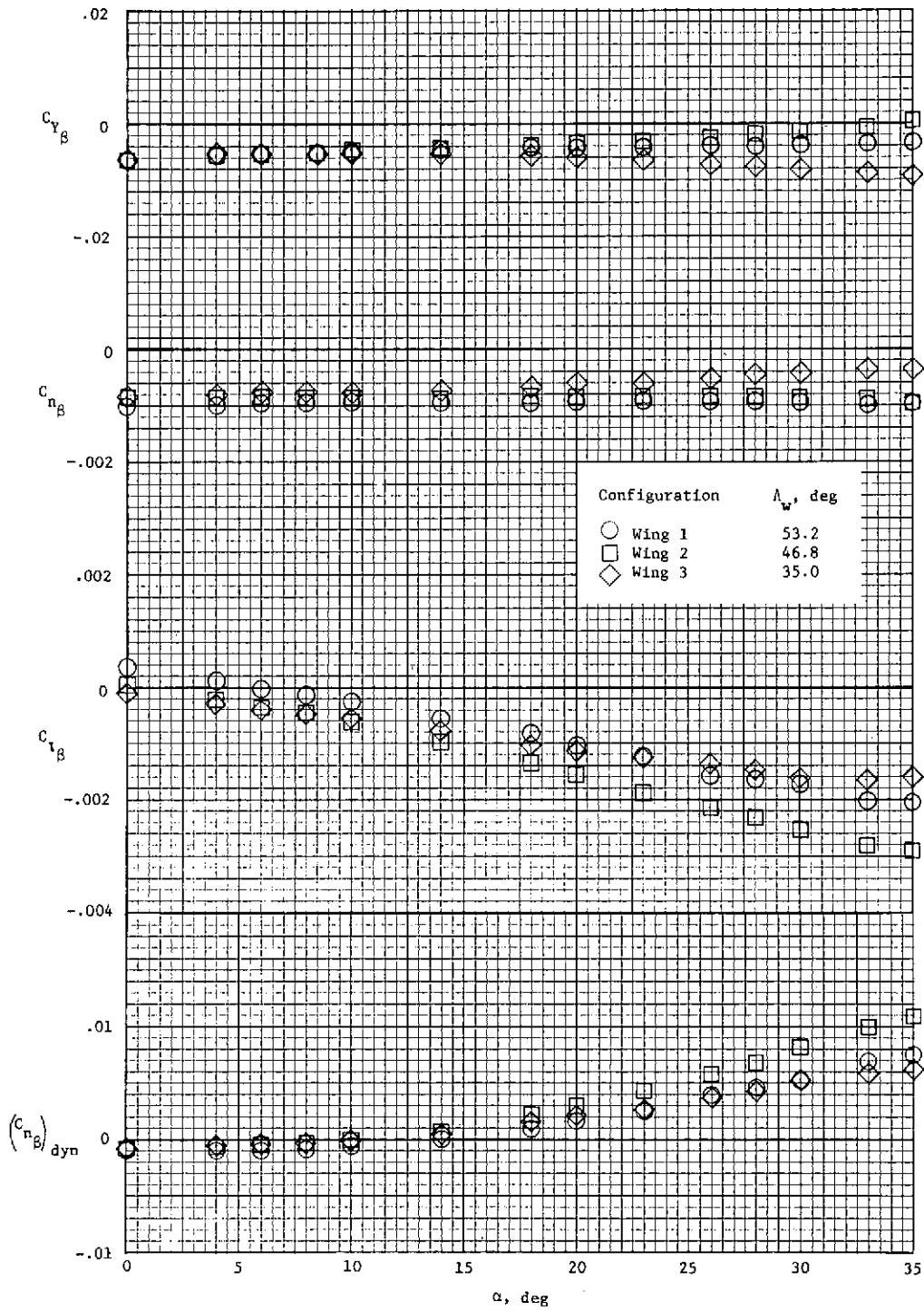
Figure 7.- Summary lateral-directional characteristics of the three wing-body combination (without fillets).
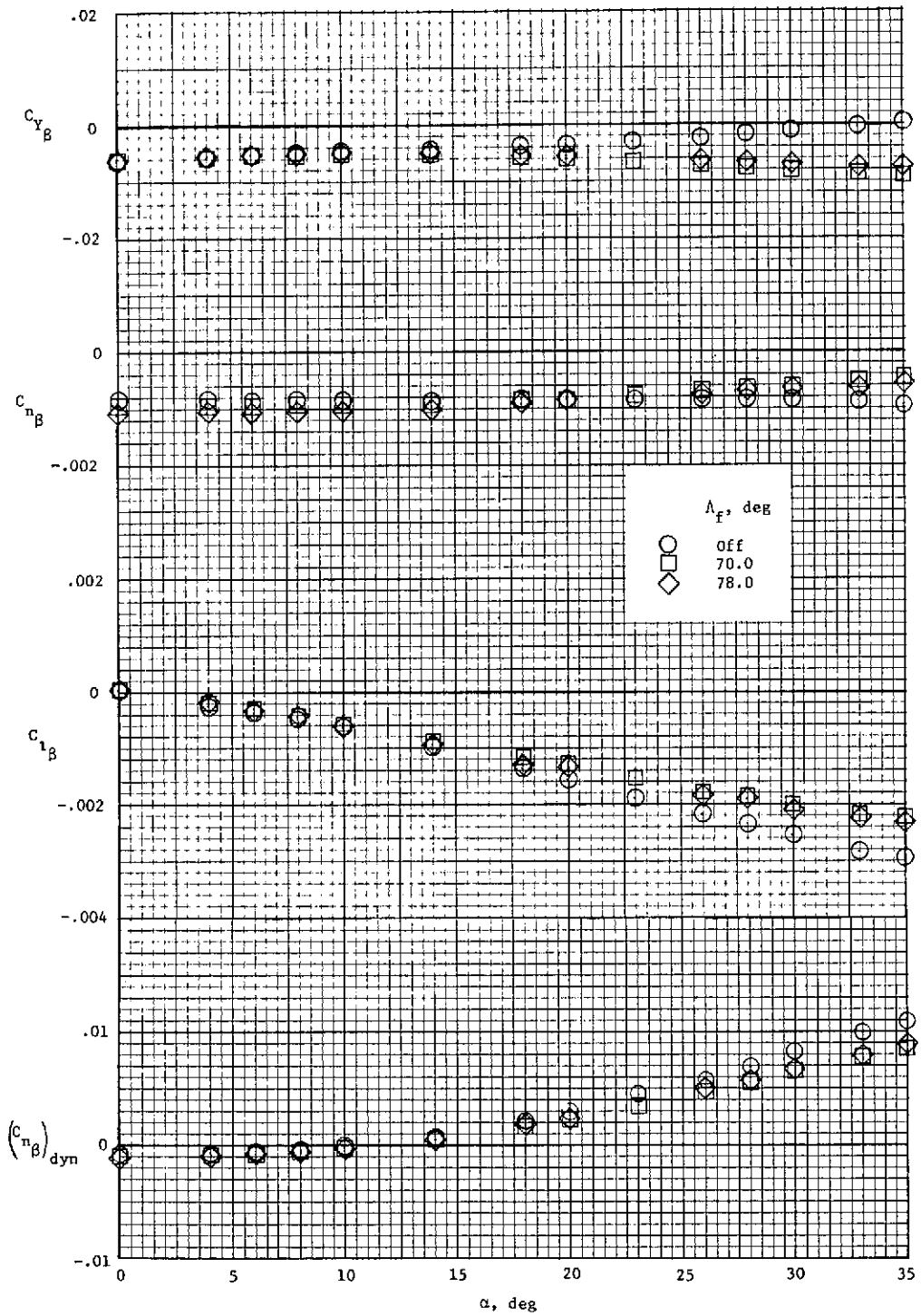
Figure 8.- Effect of fillets on lateral-directional characteristics of the body plus wing 2.
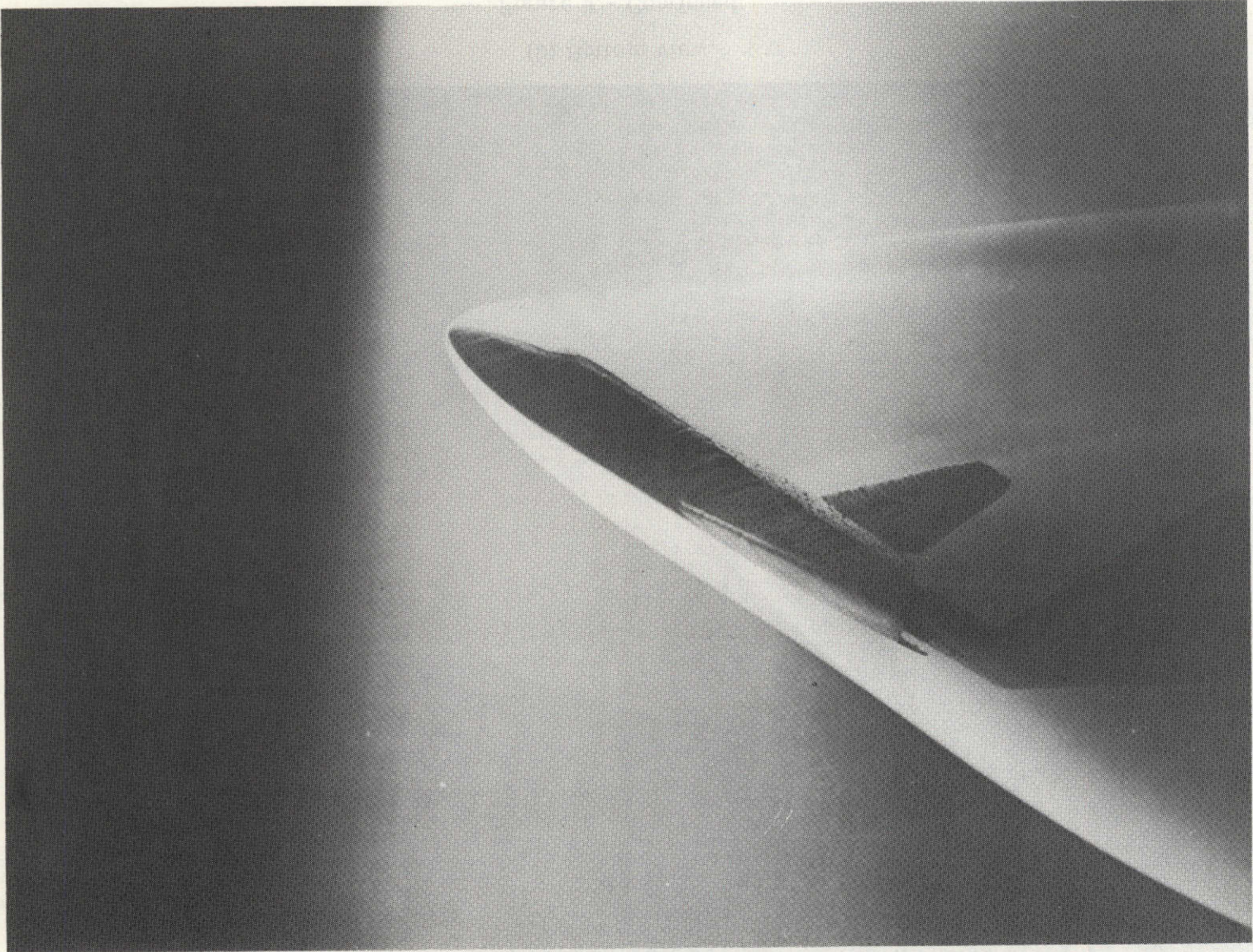
(a) Side view.

Figure 9.- Electron-beam and oil flow using wing 2. $\alpha = 30^{\circ}$.
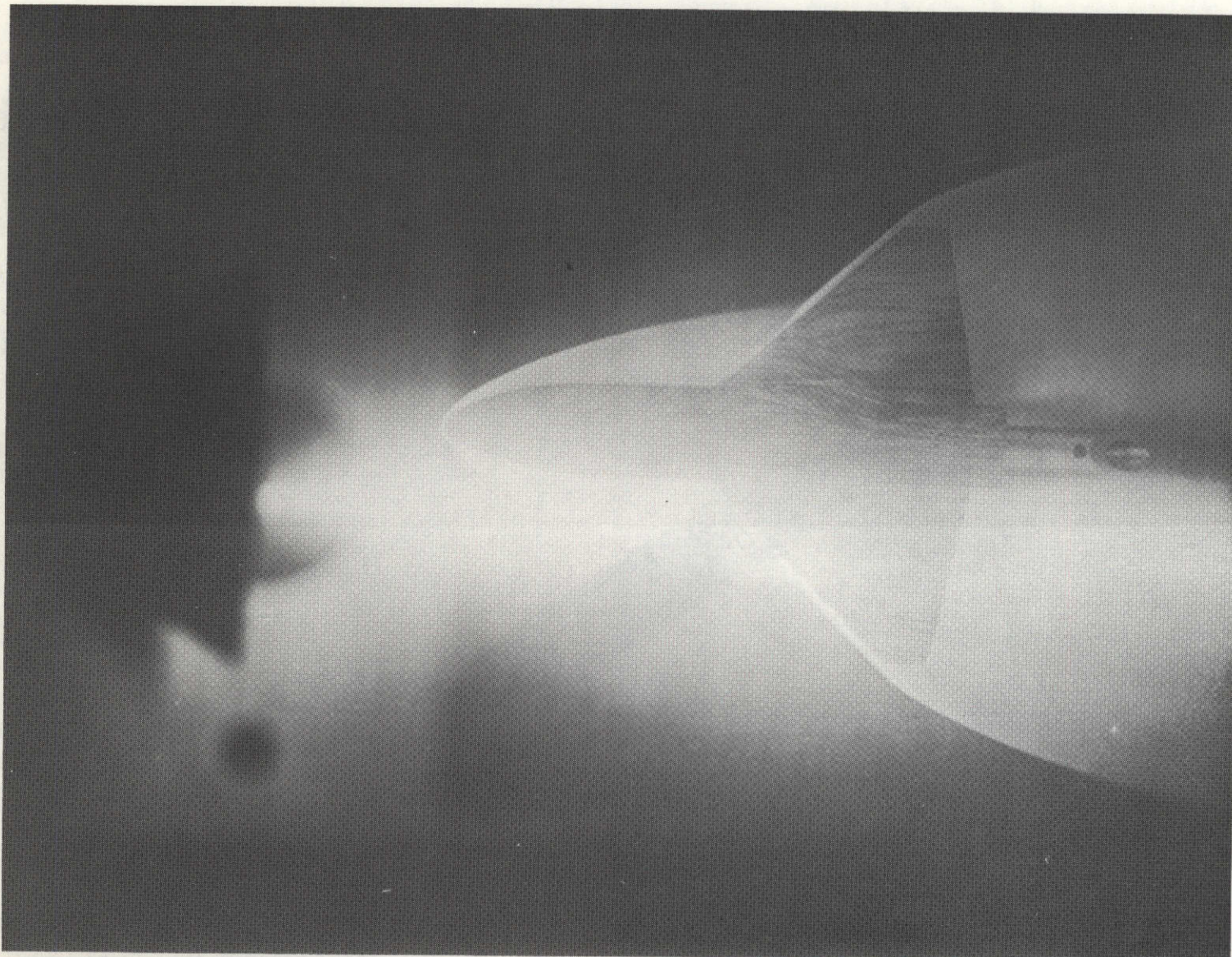
L-73-2662

(b) Bottom view.

L-73-2661

Figure 9.- Continued.
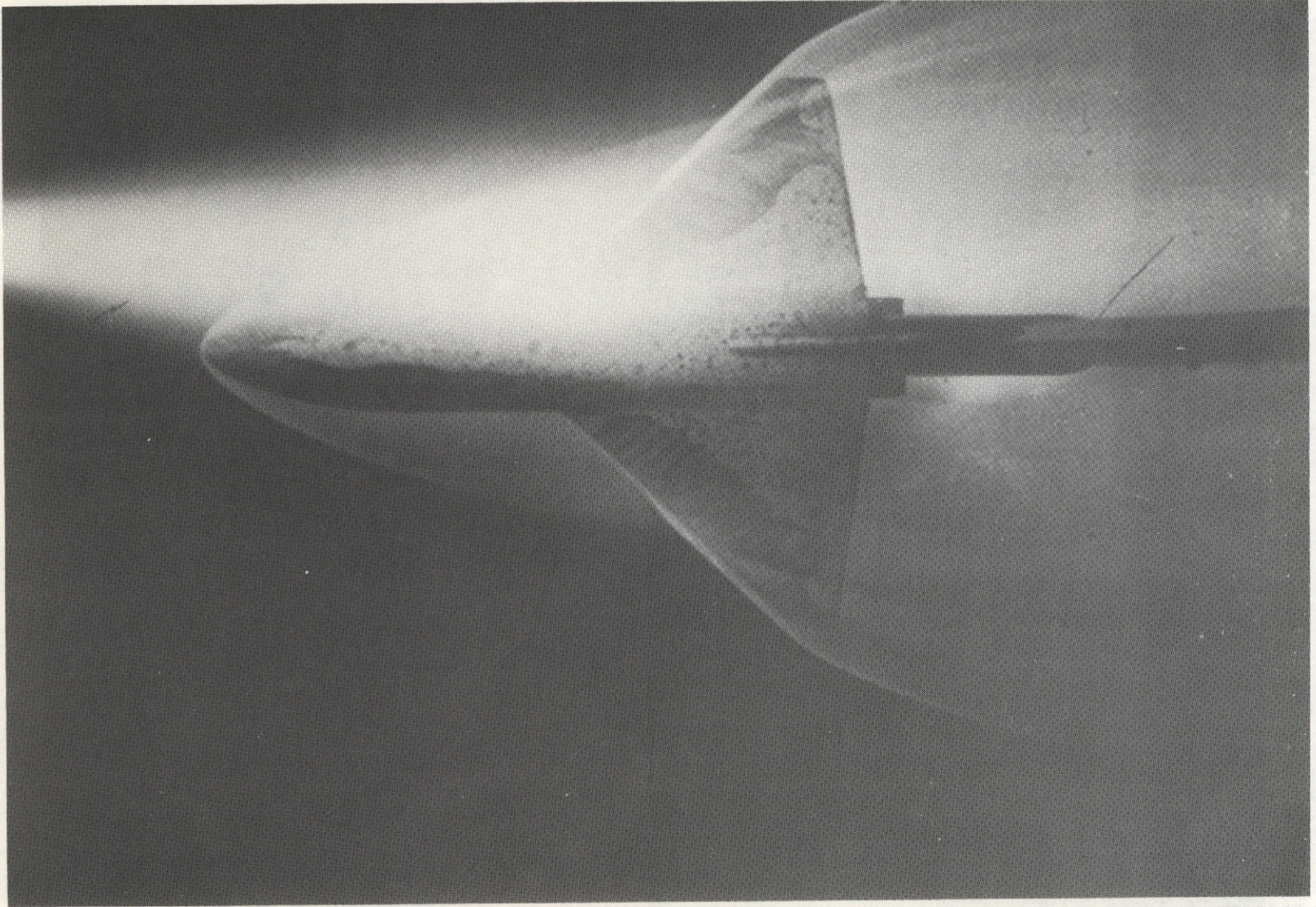
(c) Top view.

Figure 9.- Concluded.
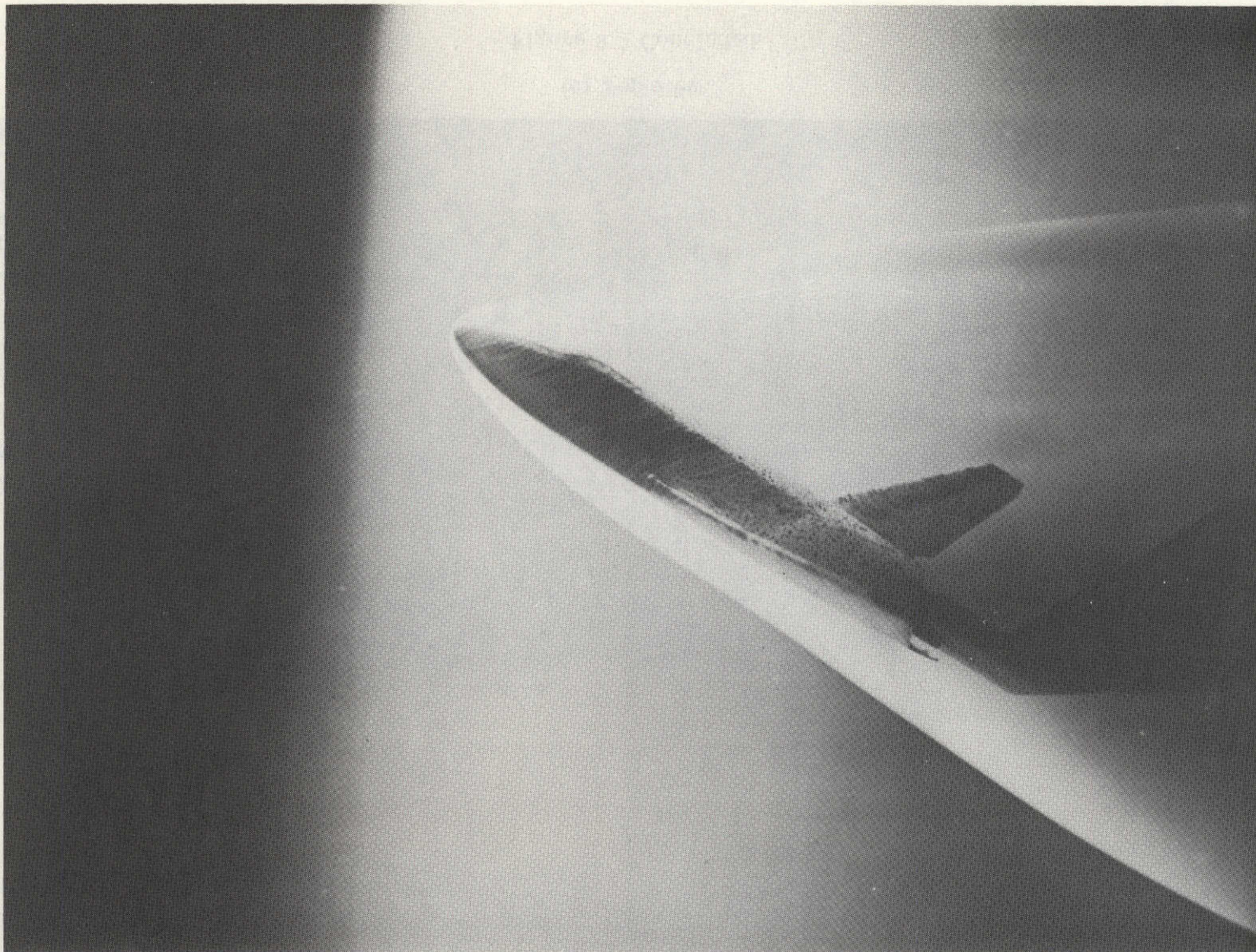
(a) Side view.

L-73-2657

Figure 10.- Electron beam and oil flow using wing 2 with 65° fillet. $\alpha = 30^O$.
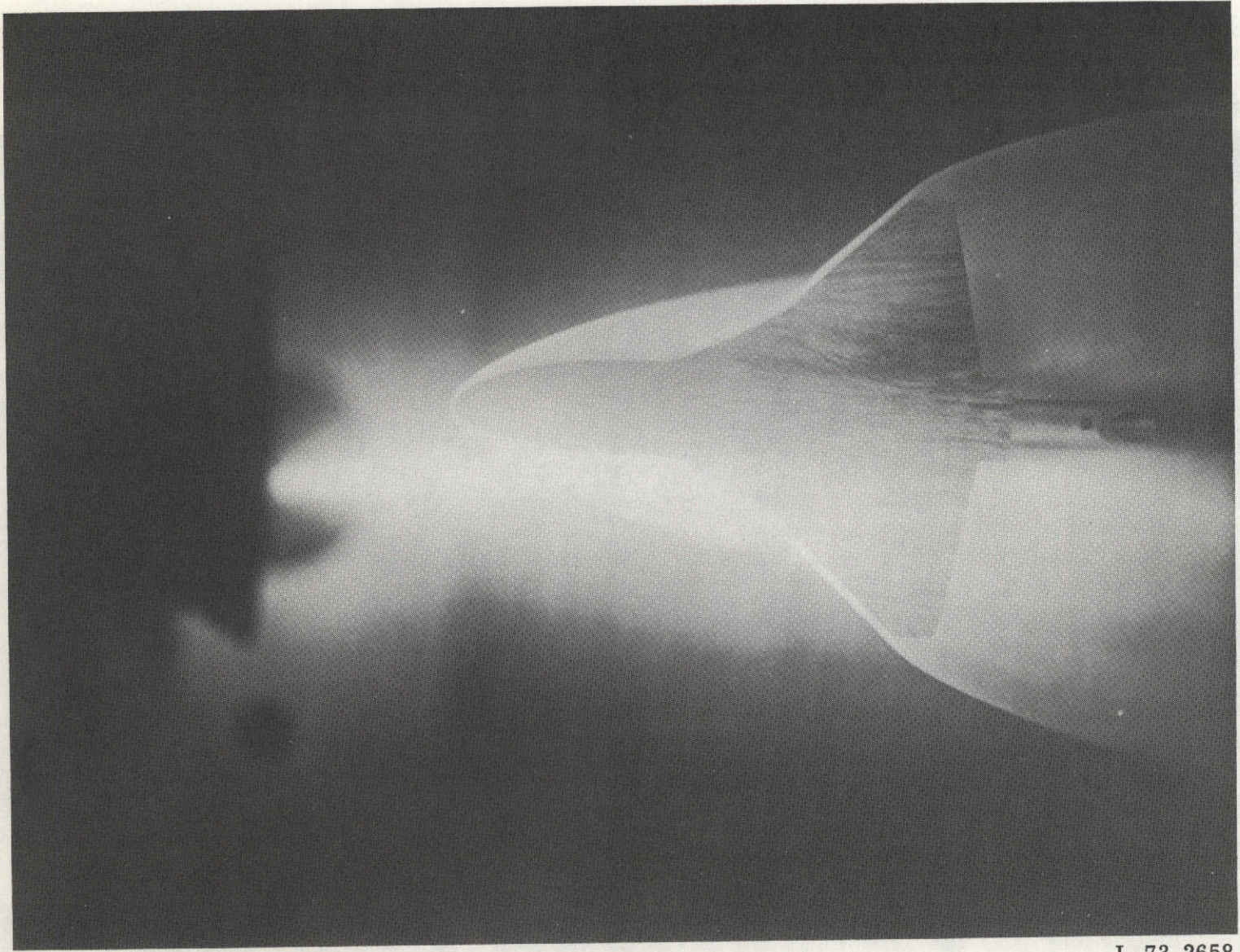
(b) Bottom view.

Figure 10.- Continued.
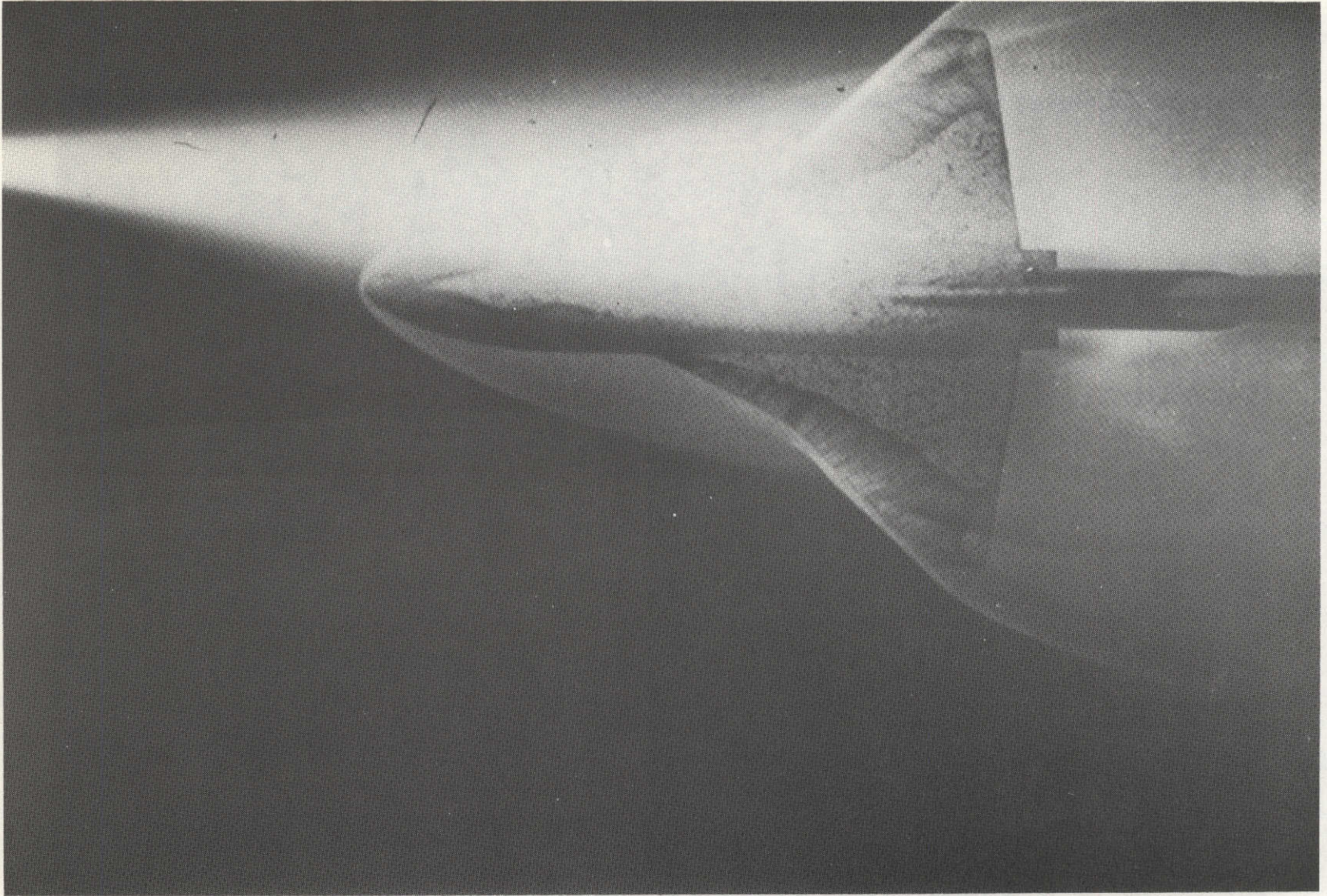
L-73-2658

(c) Top view.

L-74-1093

Figure 10.- Concluded.
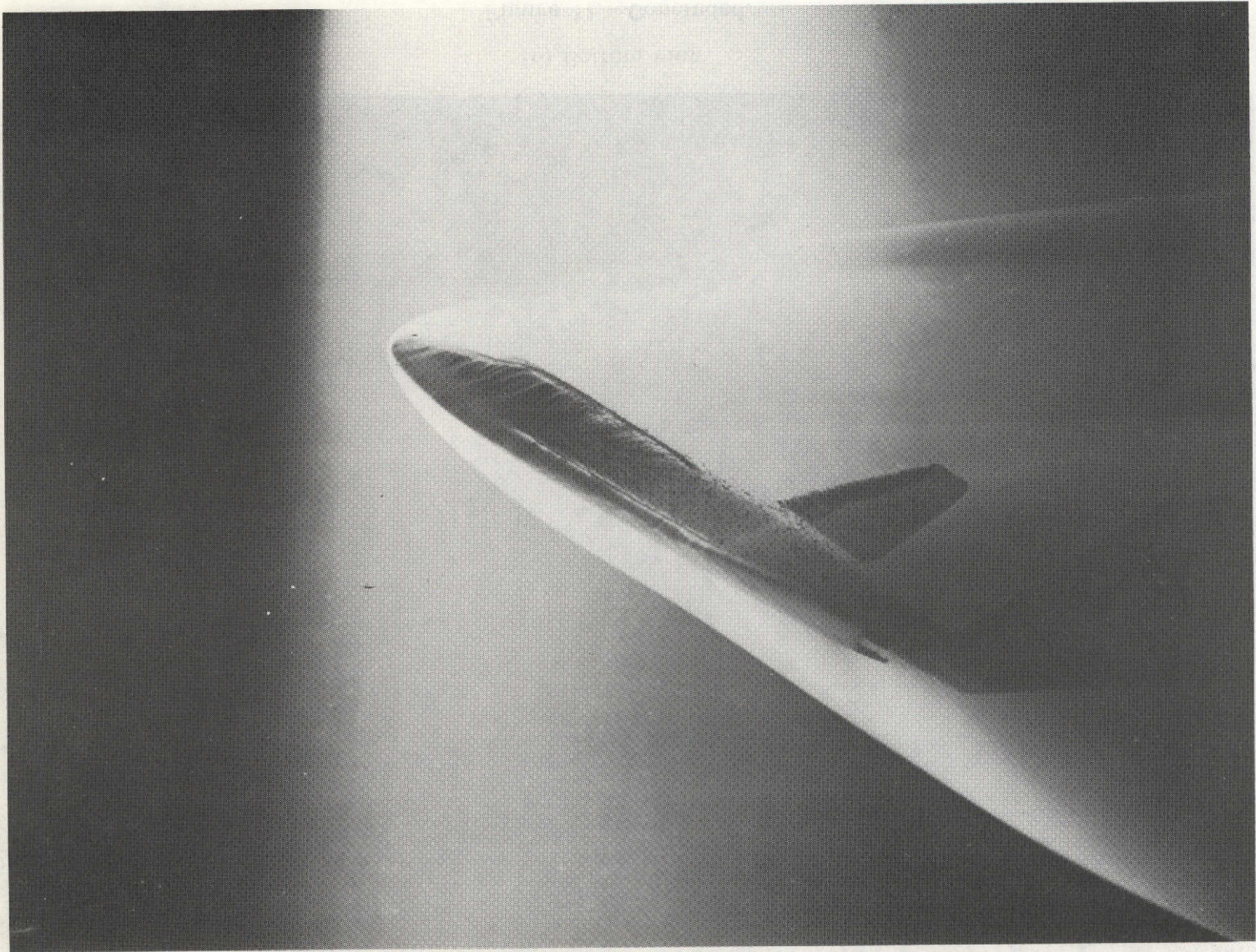
L-73-2655

(a) Side view.

Figure 11.- Electron beam and oil flow using wing 2 with 78° fillet. $\alpha = 30^\circ$.
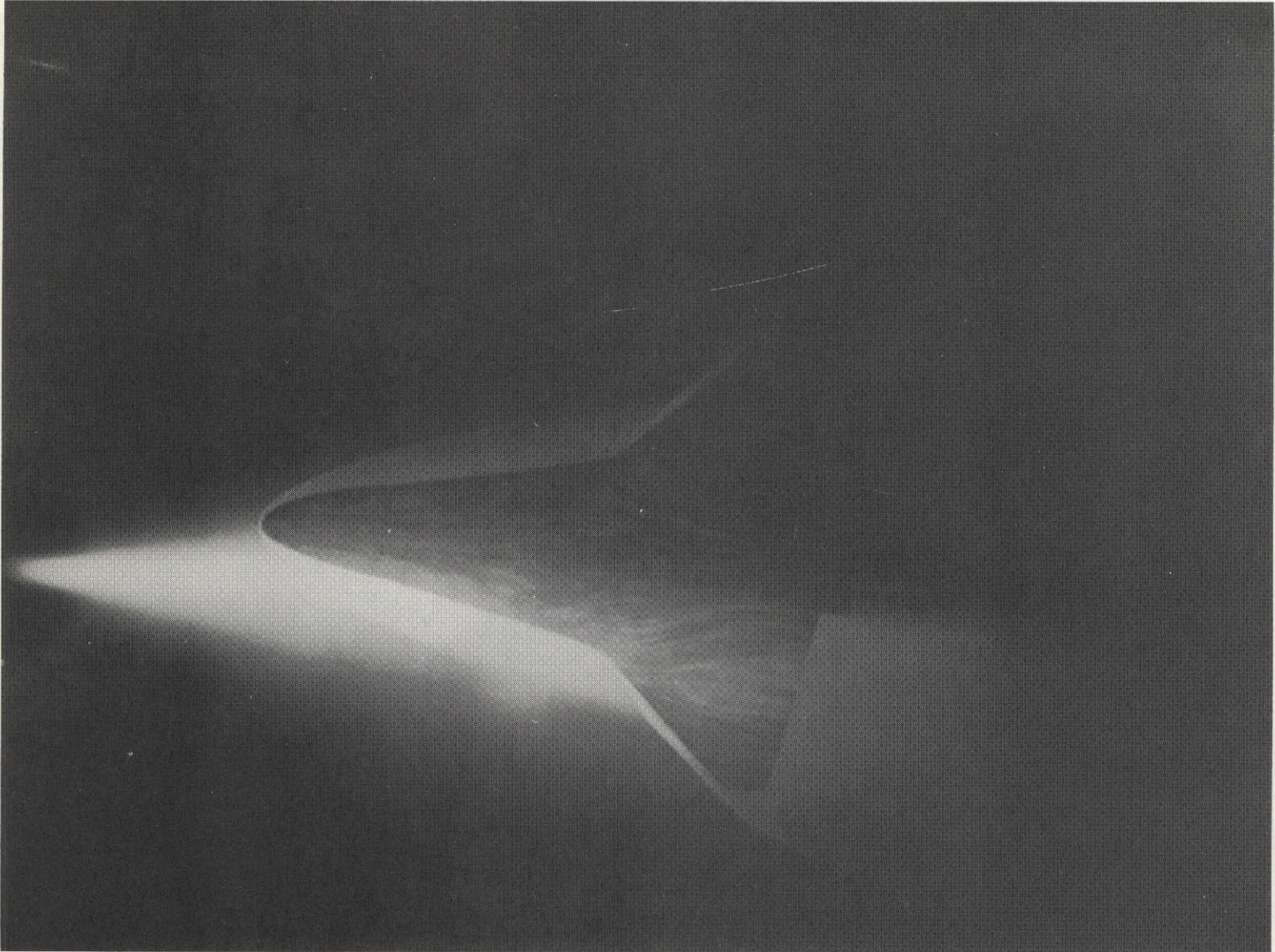
(b) Bottom view.

Figure 11.- Concluded.
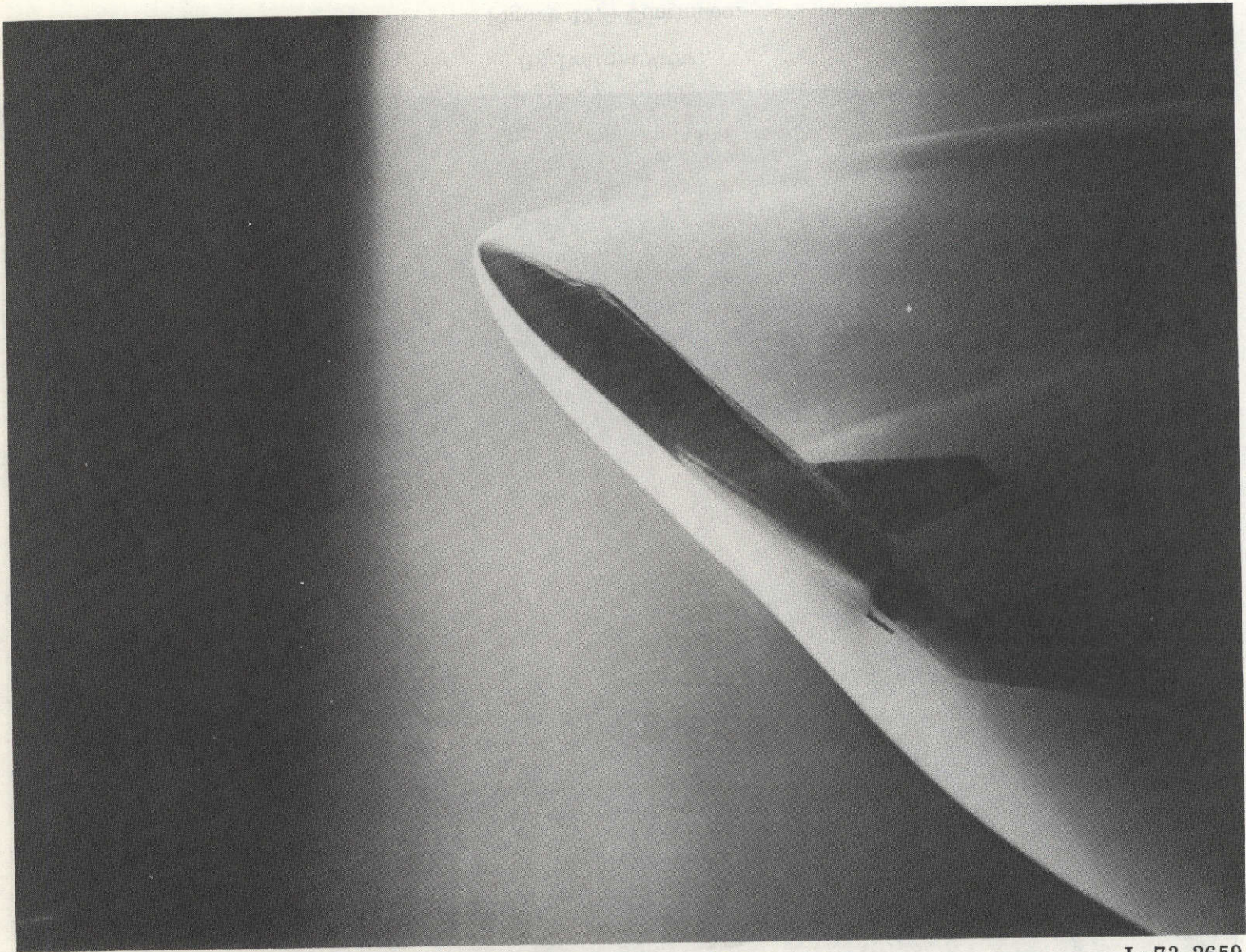
L-73-2656

L-73-2659

(a) Side view.

Figure 12.- Electron beam and oil flow using wing 2. $\alpha = 40^O$.
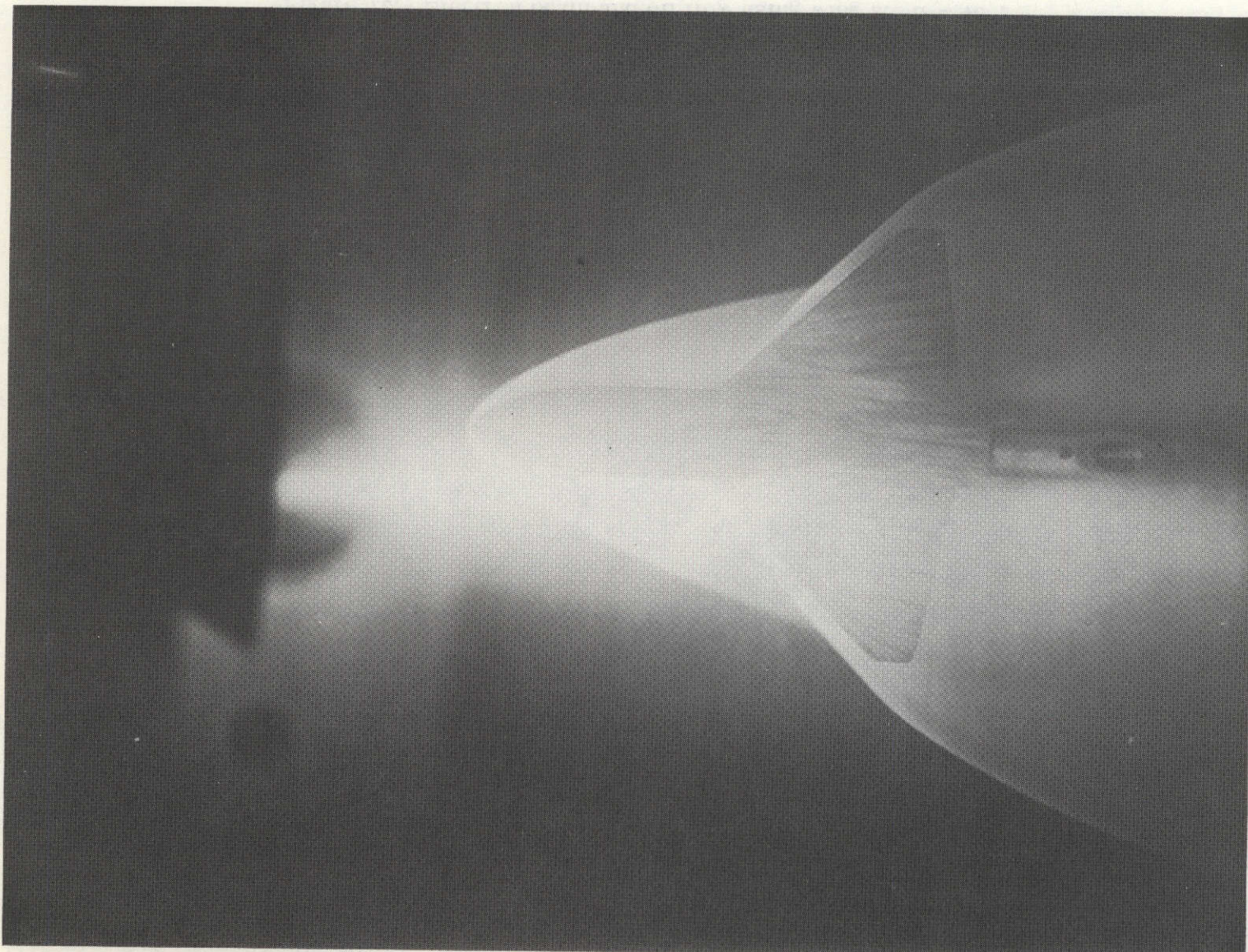
(b) Bottom view.

L-73-2660

Figure 12.- Continued.
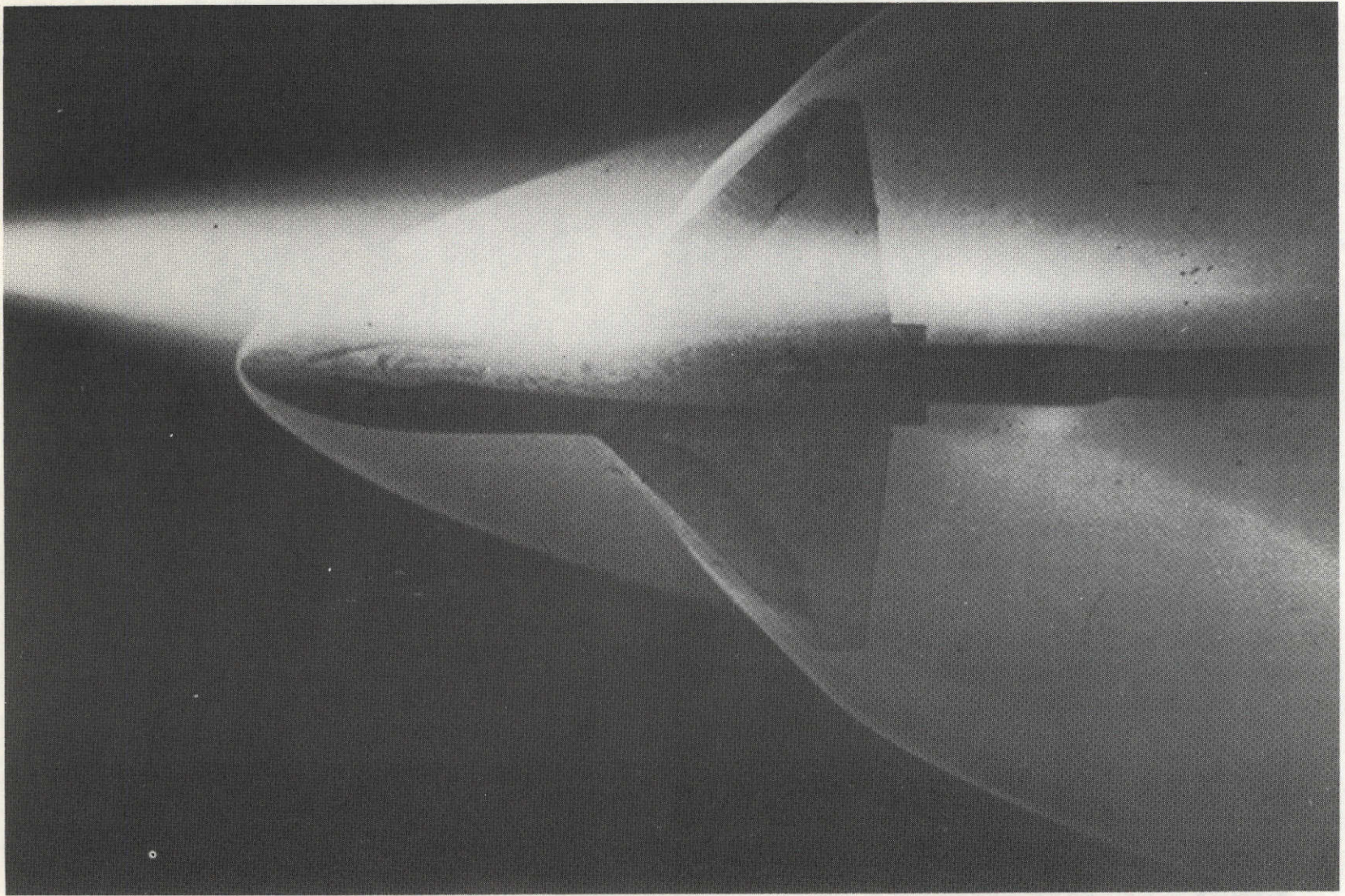
(c) Top view.

Figure 12.- Concluded.
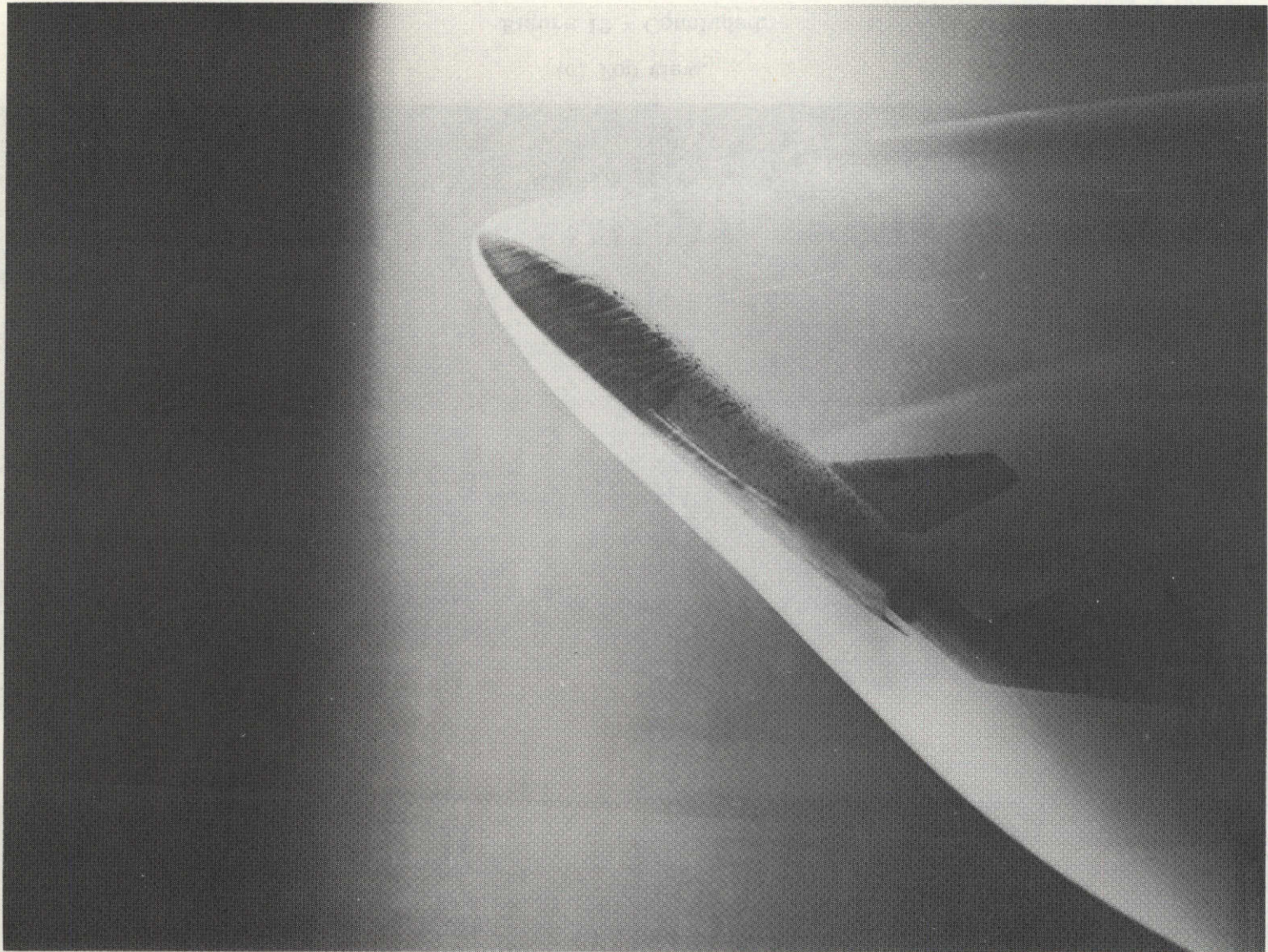
L-74-1094

(a) Side view.

L-73-2663

Figure 13.- Electron beam and oil flow using wing 2 with 65° fillet. $\alpha = 40^O$.
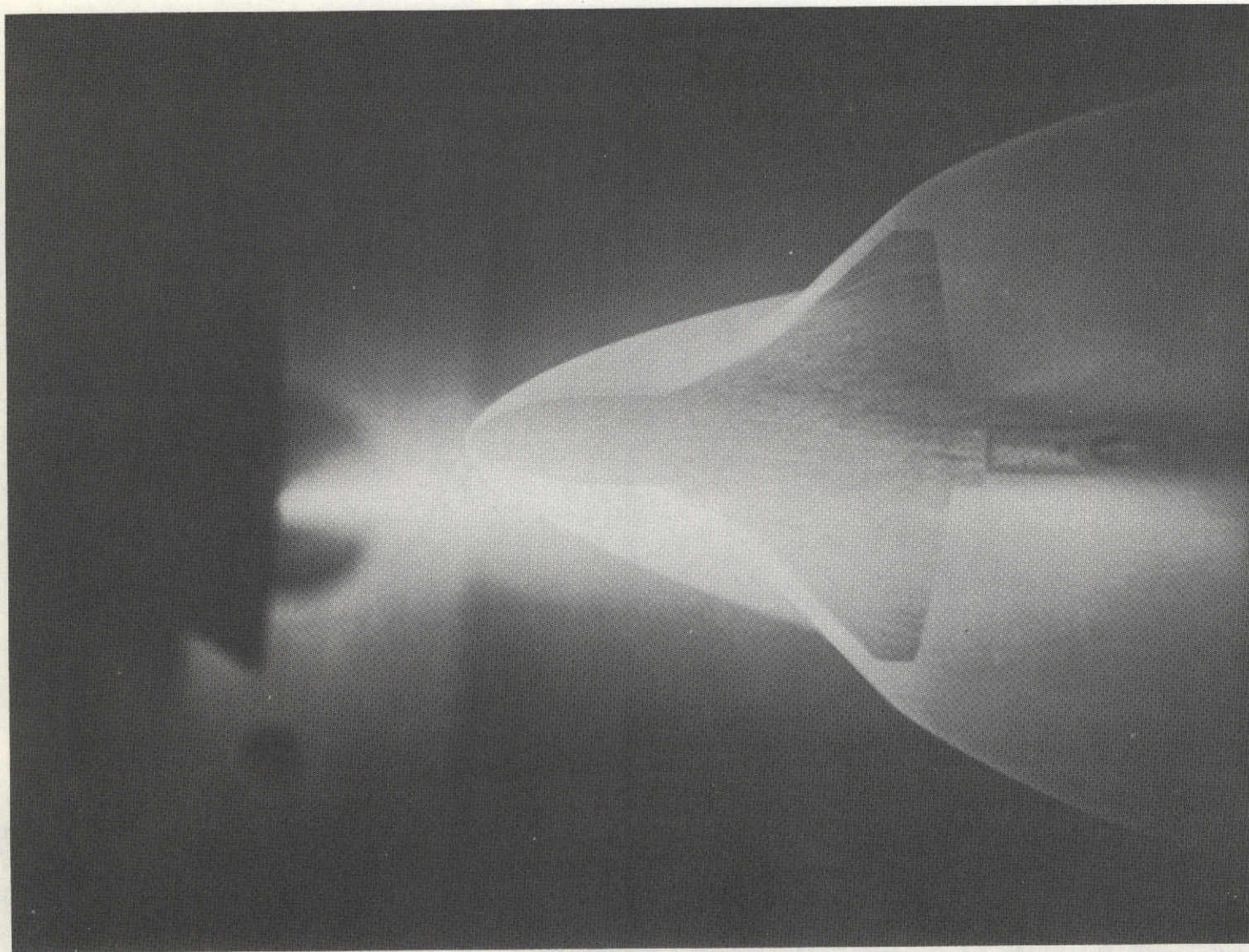
(b) Bottom view.

L-73-2664

Figure 13.- Continued.
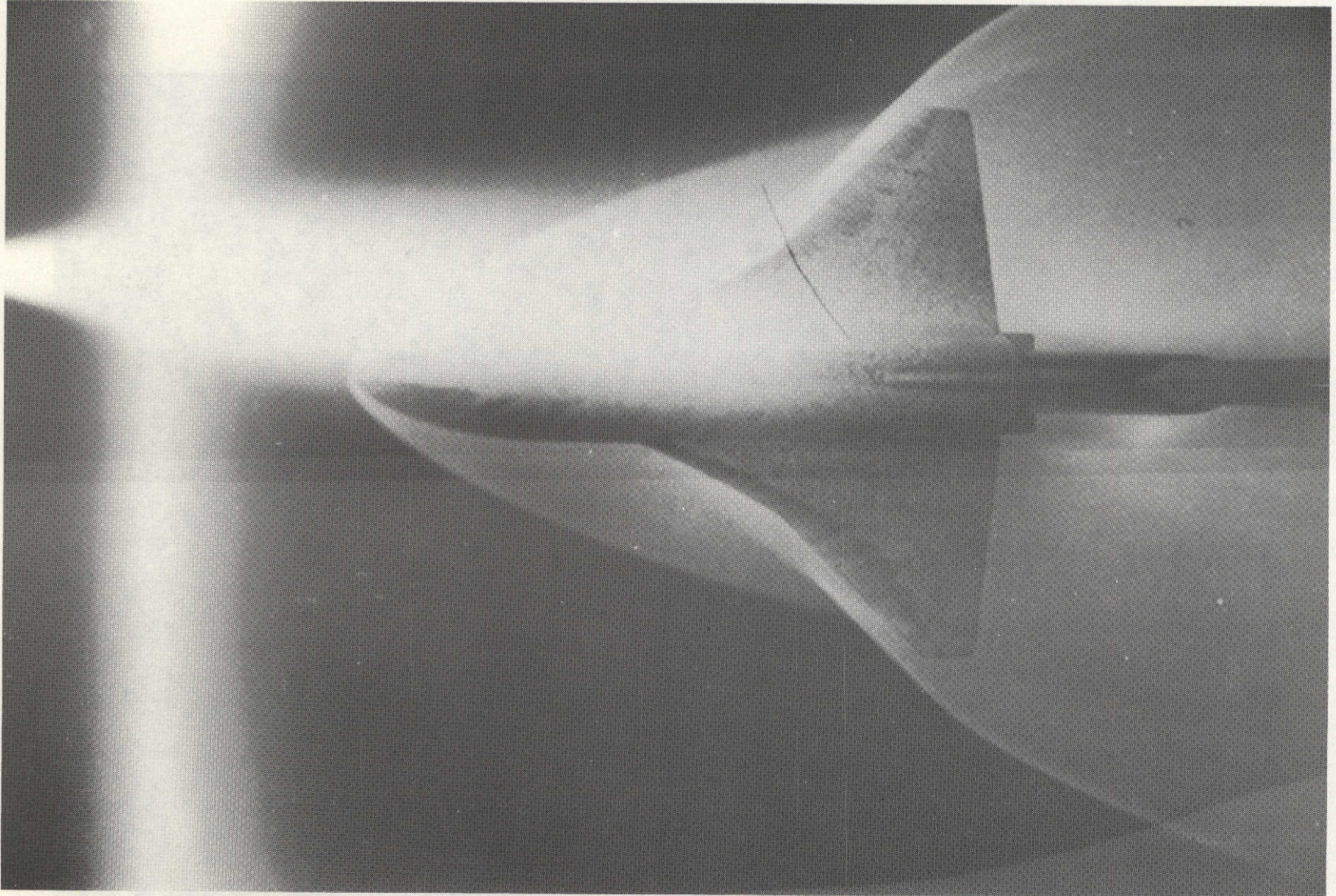
(c) Top view.

L-74-1095

Figure 13.- Concluded.
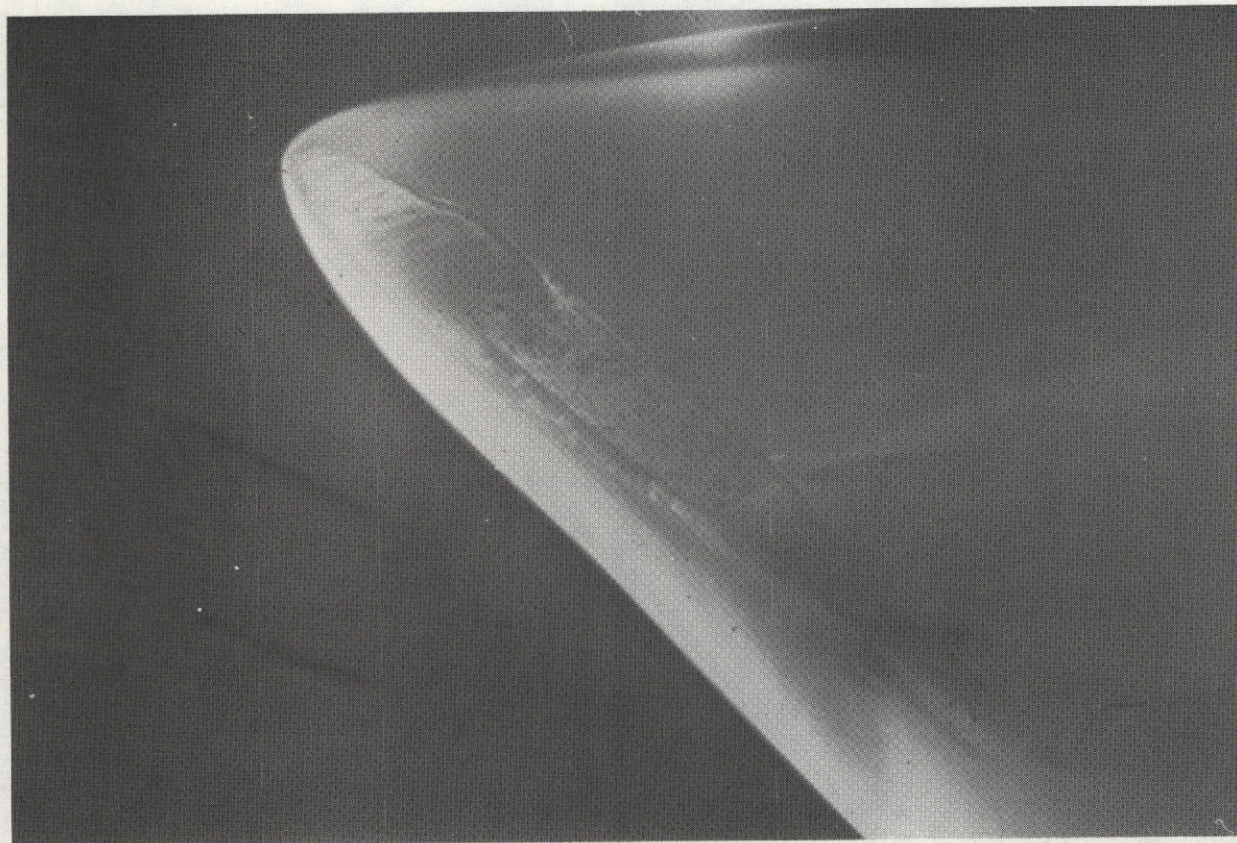
L-74-1096

(a) Side view.

Figure 14.- Electron beam and oil flow using wing 2 with 78° fillet. $\alpha = 40°$.
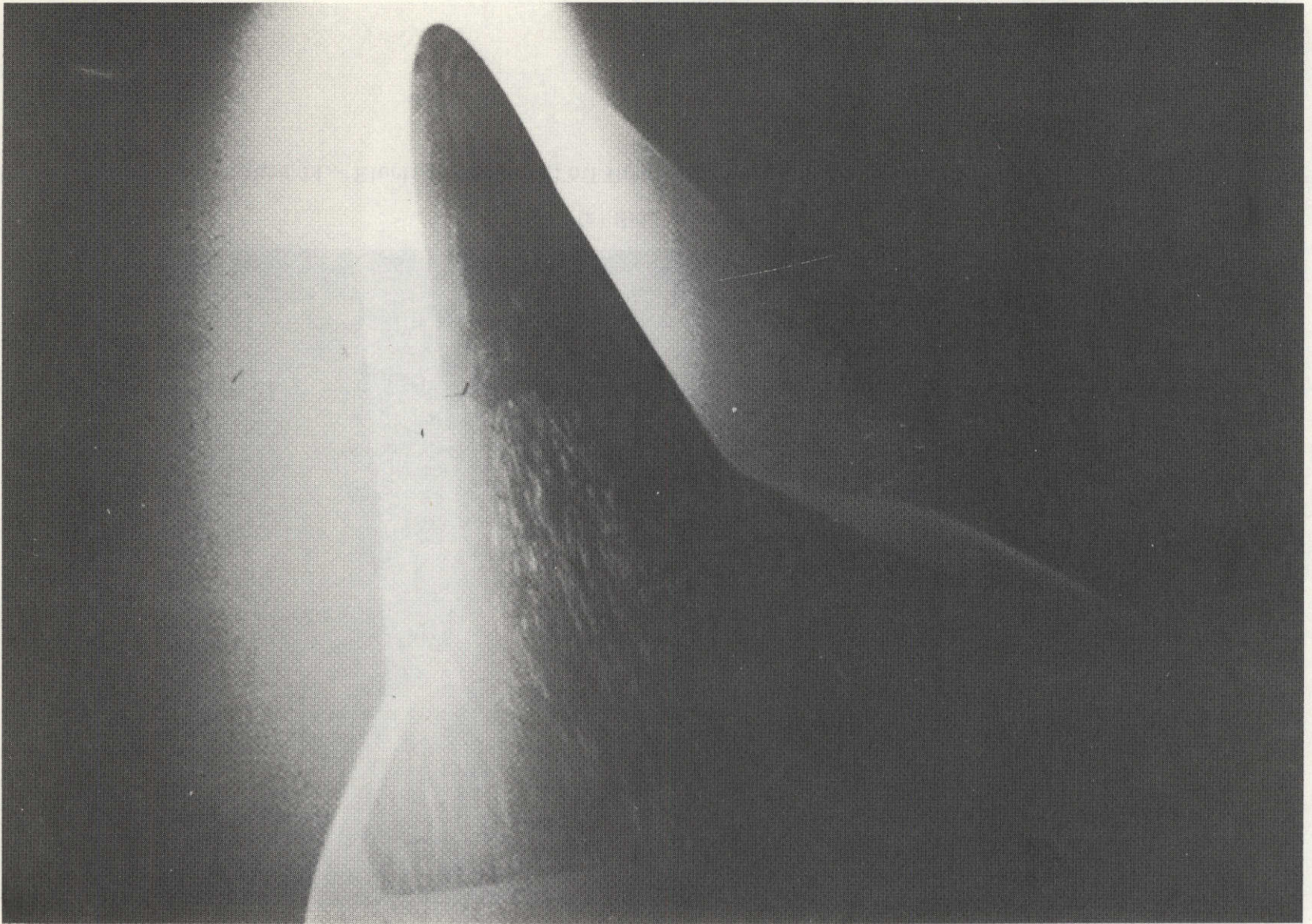
(b) Bottom view.

L-74-1097

Figure 14.- Concluded.
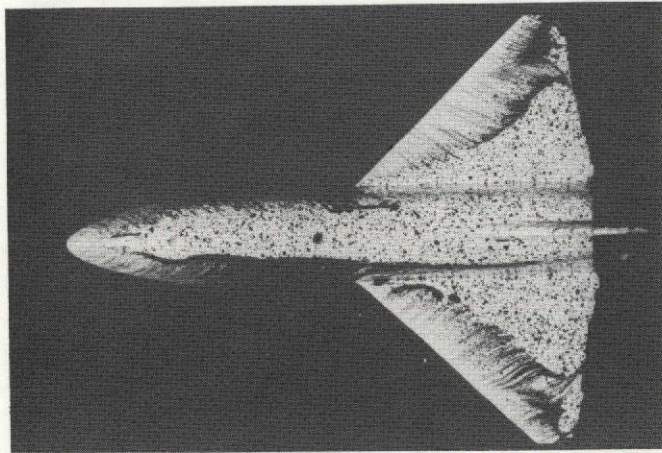
(a) Top view.
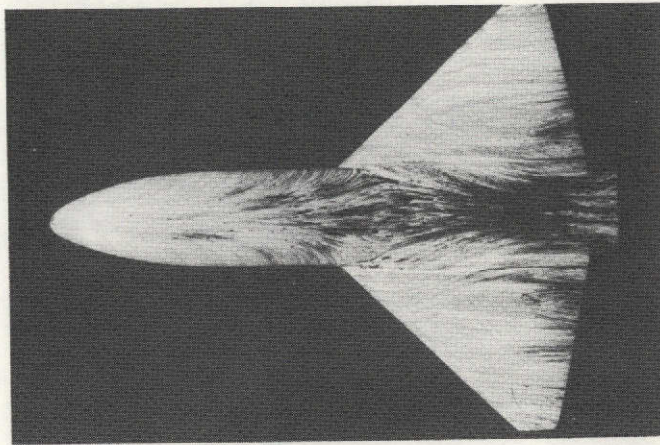
(b) Bottom view.
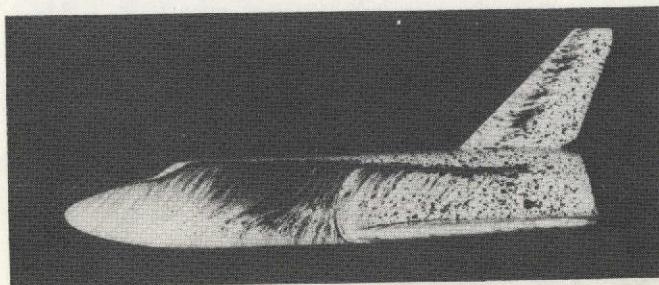
(c) Side view.   L-74-1098

Figure 15.- Surface oil flow using wing 2. $\alpha = 30^O$.
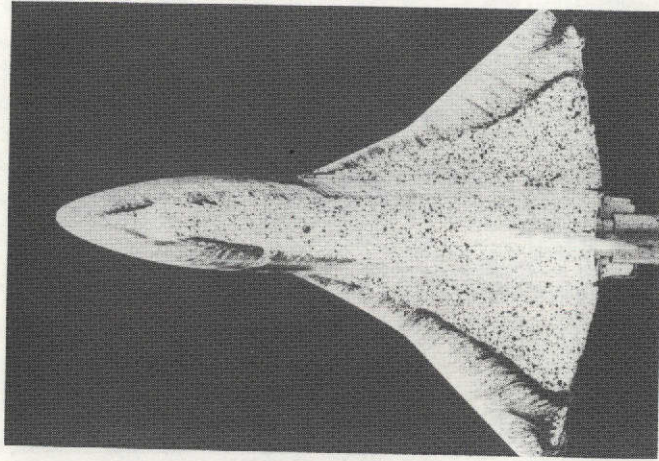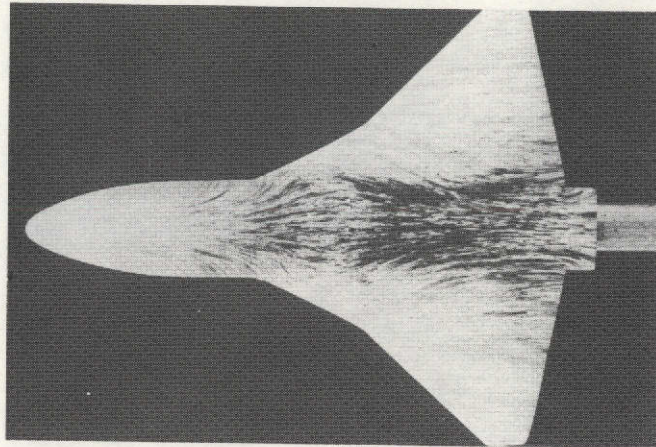
(a) Top view.
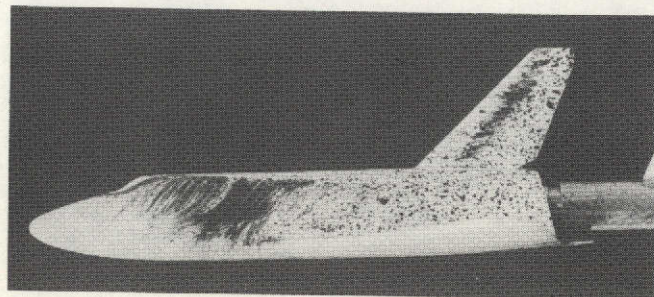
(b) Bottom view.

(c) Side view.   L-74-1099

Figure 16.- Surface oil flow using wing 2 with 65° fillet. α = 30°.
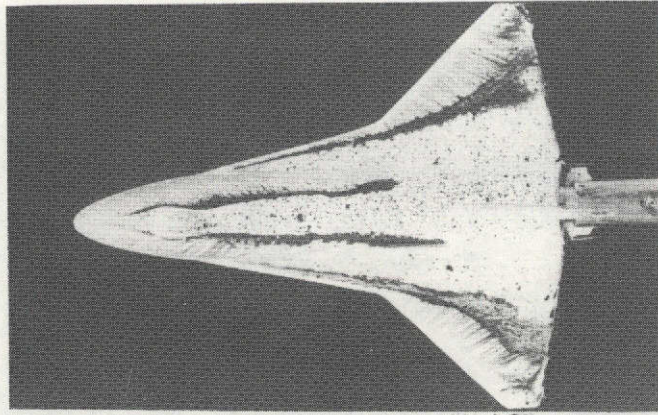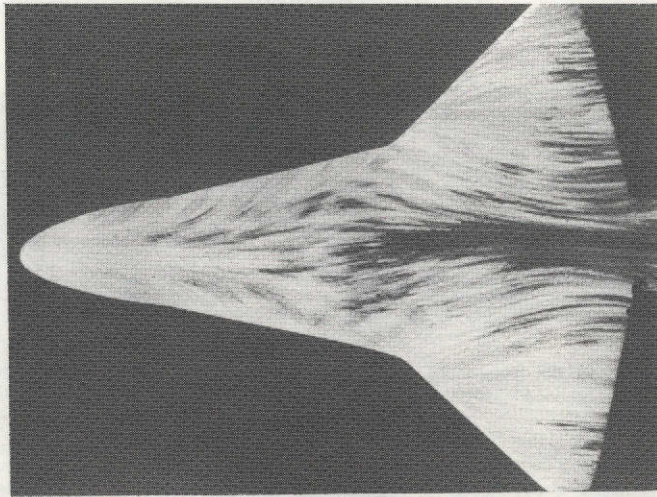
(a) Top view.
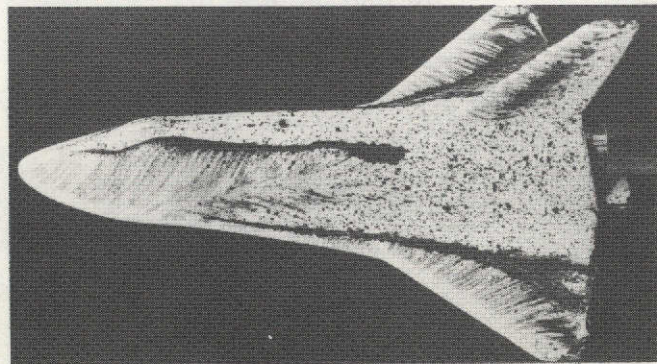
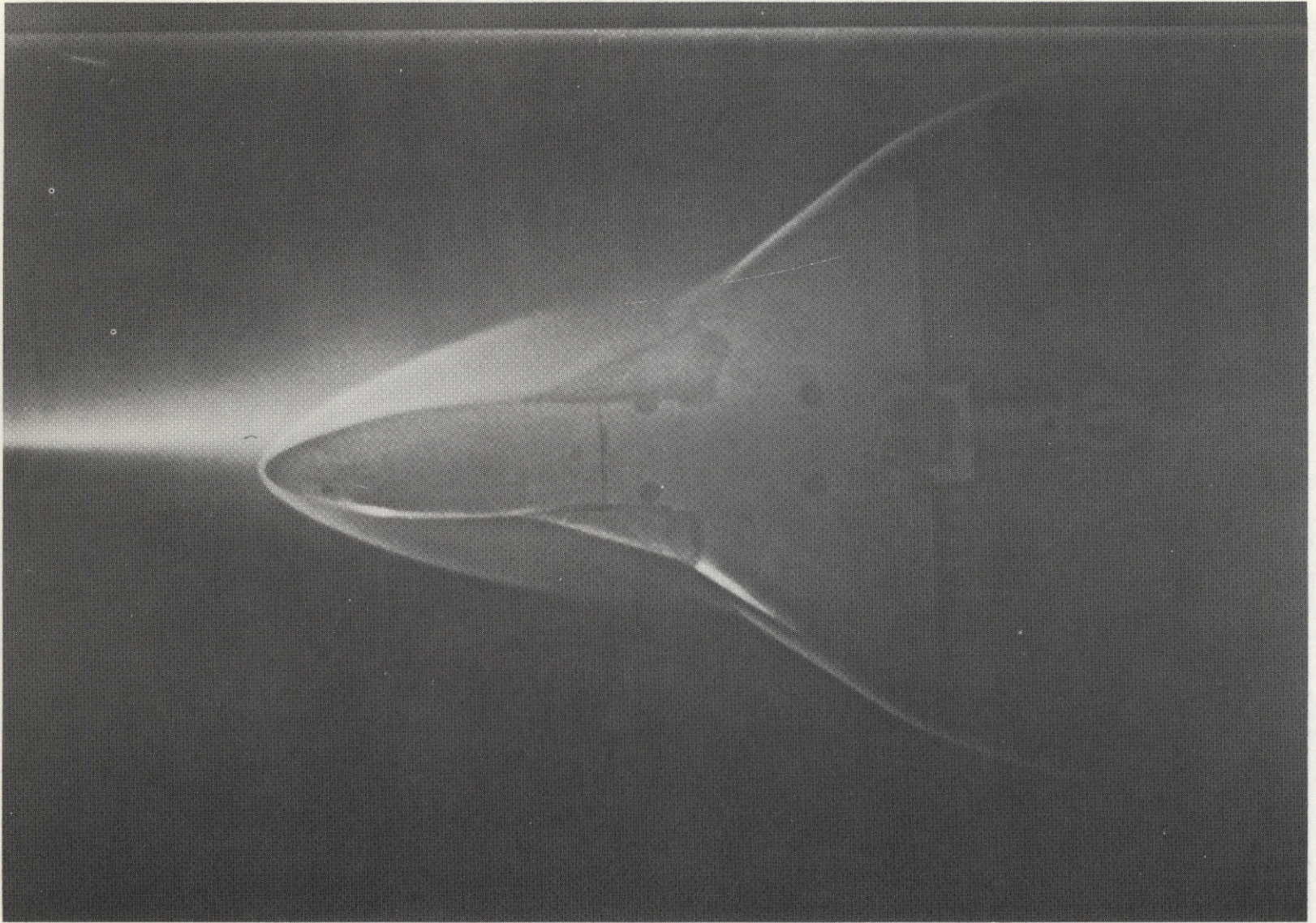
(b) Bottom view.

(c) Side view.   L-74-1100

Figure 17.- Surface oil flow using wing 2 with 78° fillet. α = 30°.
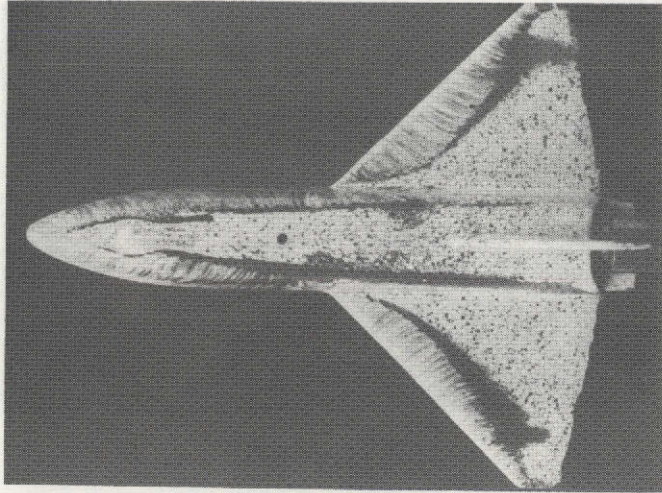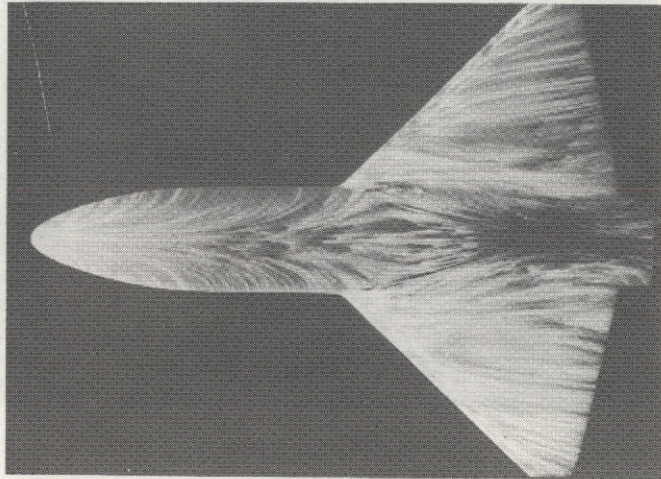
(a) Top view.
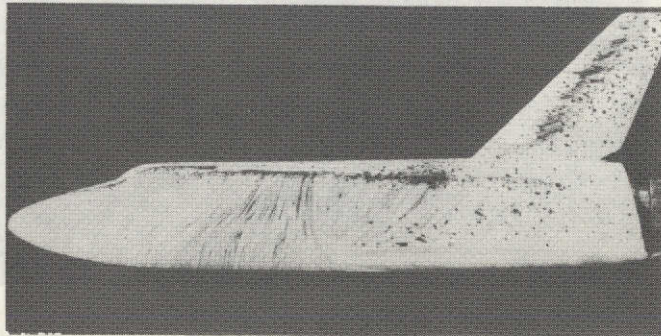
(b) Bottom view.

(c) Side view.

L-74-1101

Figure 18.- Surface oil flow using wing 2. $\alpha = 40^O$.
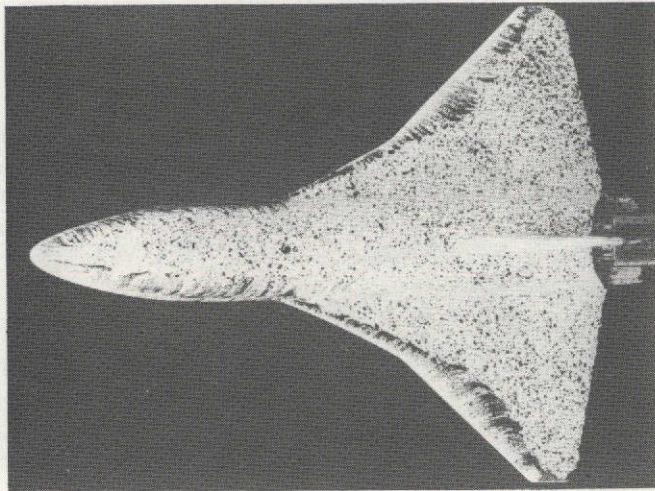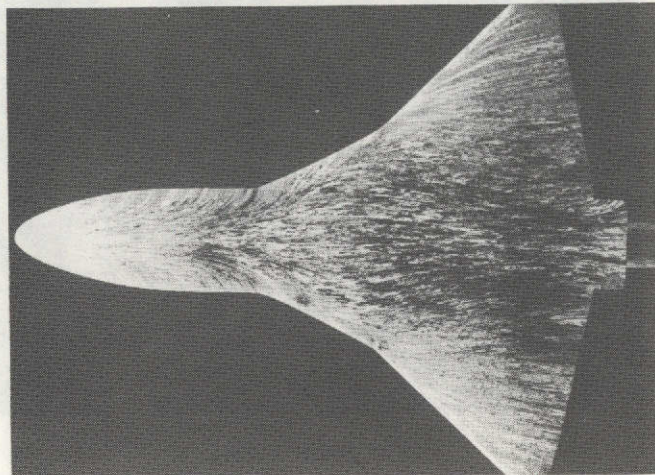
(a) Top view.
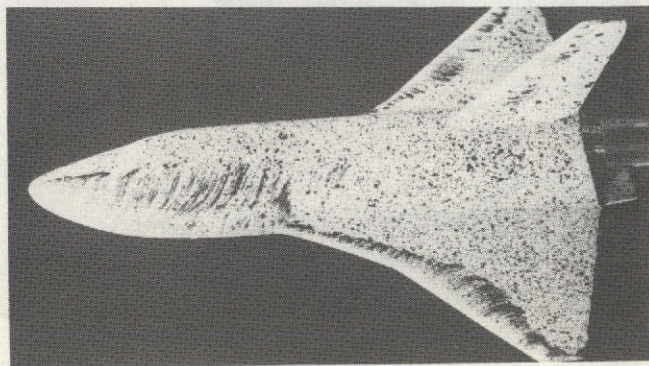
(b) Bottom view.

(c) Side view.

L-74-1102

Figure 19.- Surface oil flow using wing 2 with 65° fillet. $\alpha = 40^O$.
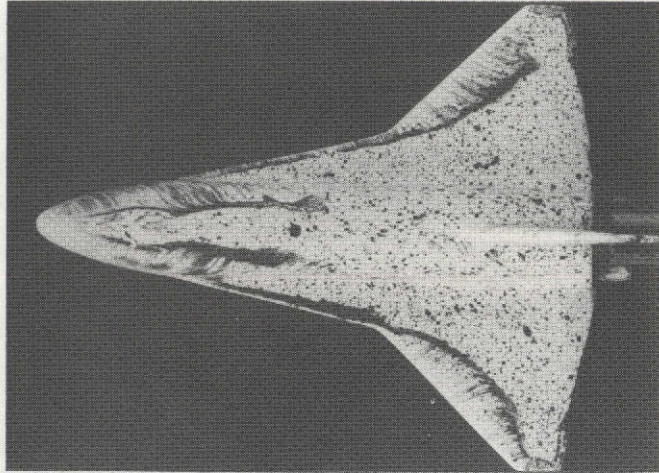
(a) Top view.
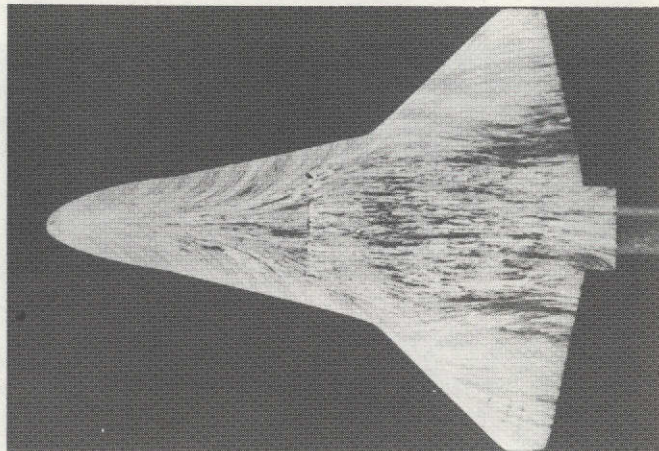
(b) Bottom view.
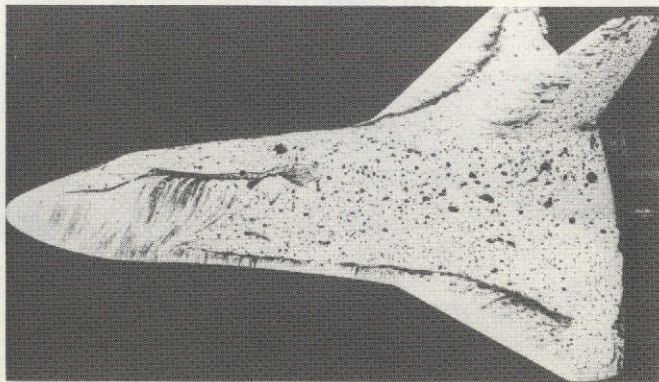
(c) Side view.

L-74-1103

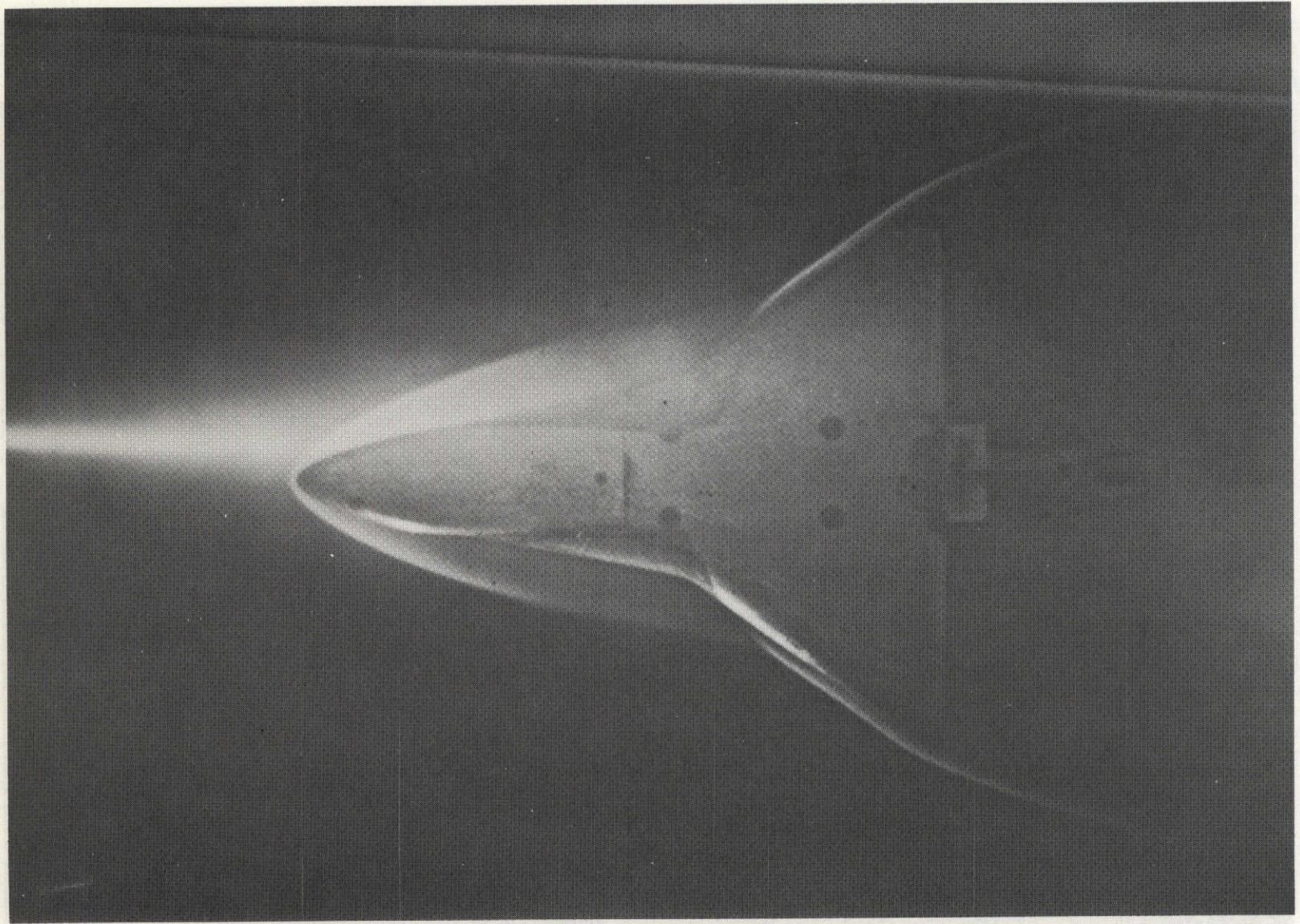Figure 20.- Surface oil flow using wing 2 with 78° fillet. $\alpha = 40^O$.
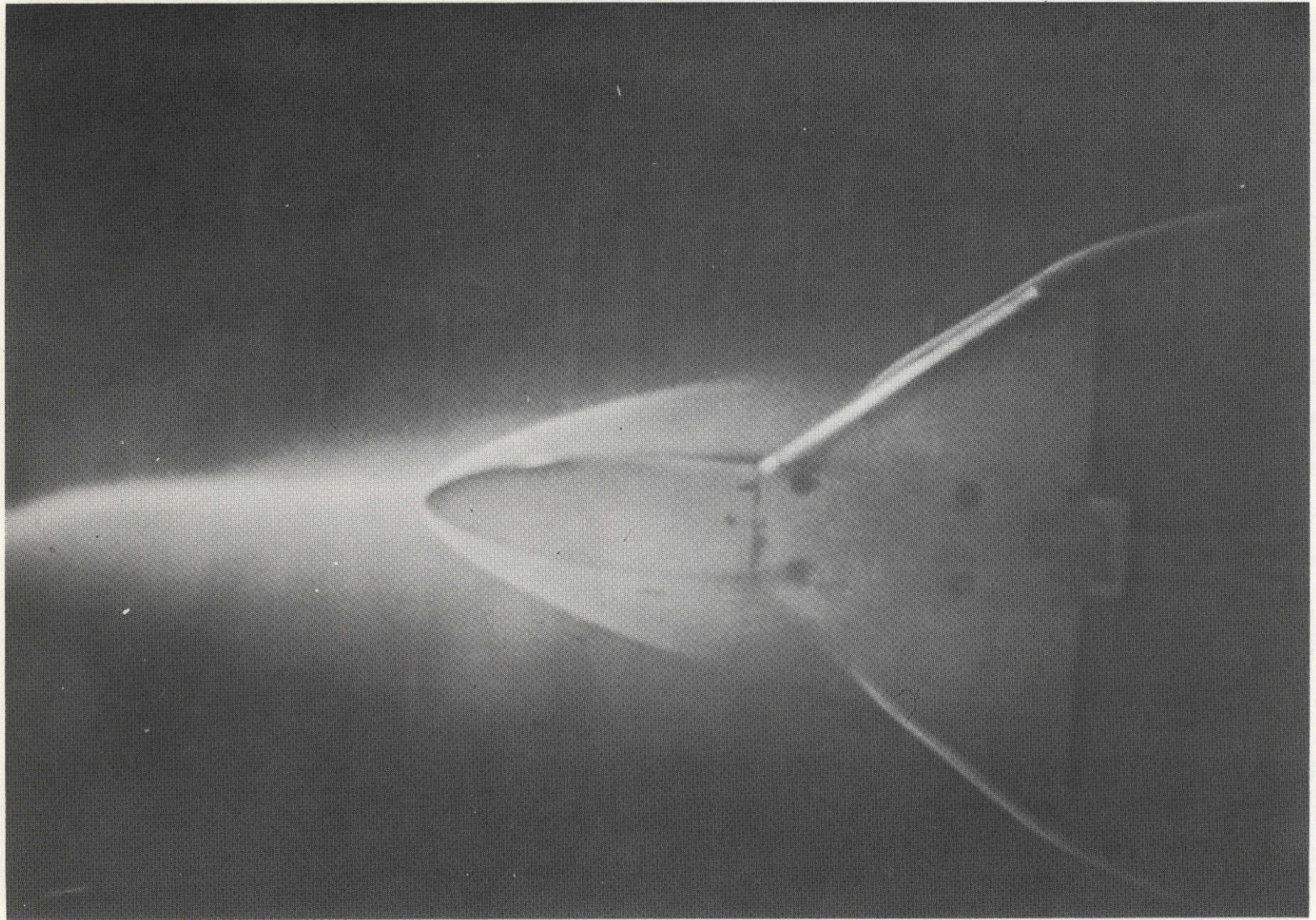
(a) Basic wing.

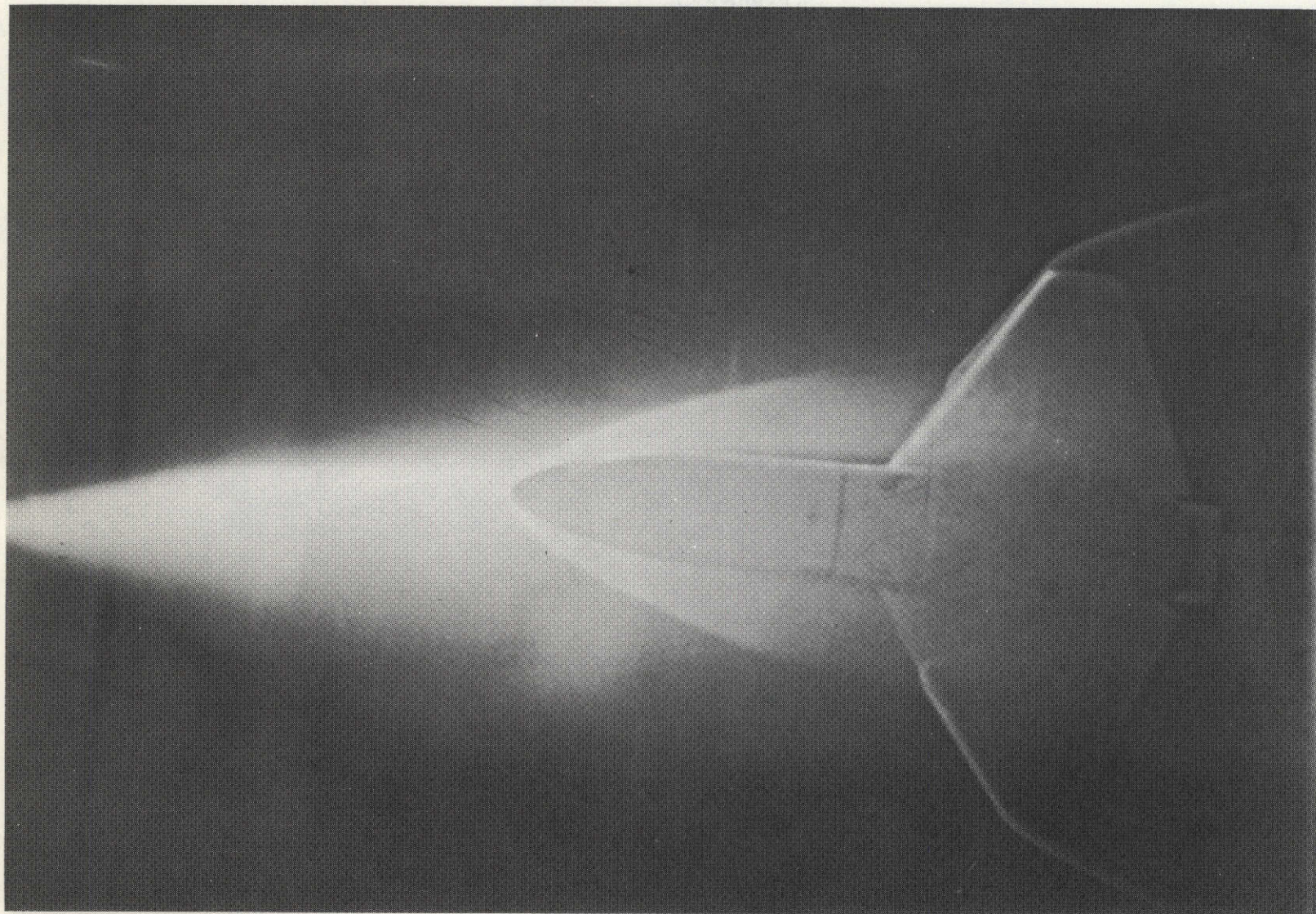Figure 21.- Electron beam using wing 1. $\alpha = 30^{\circ}$.

(b) 70° fillet.

Figure 21.- Continued.

(c) 78° fillet.
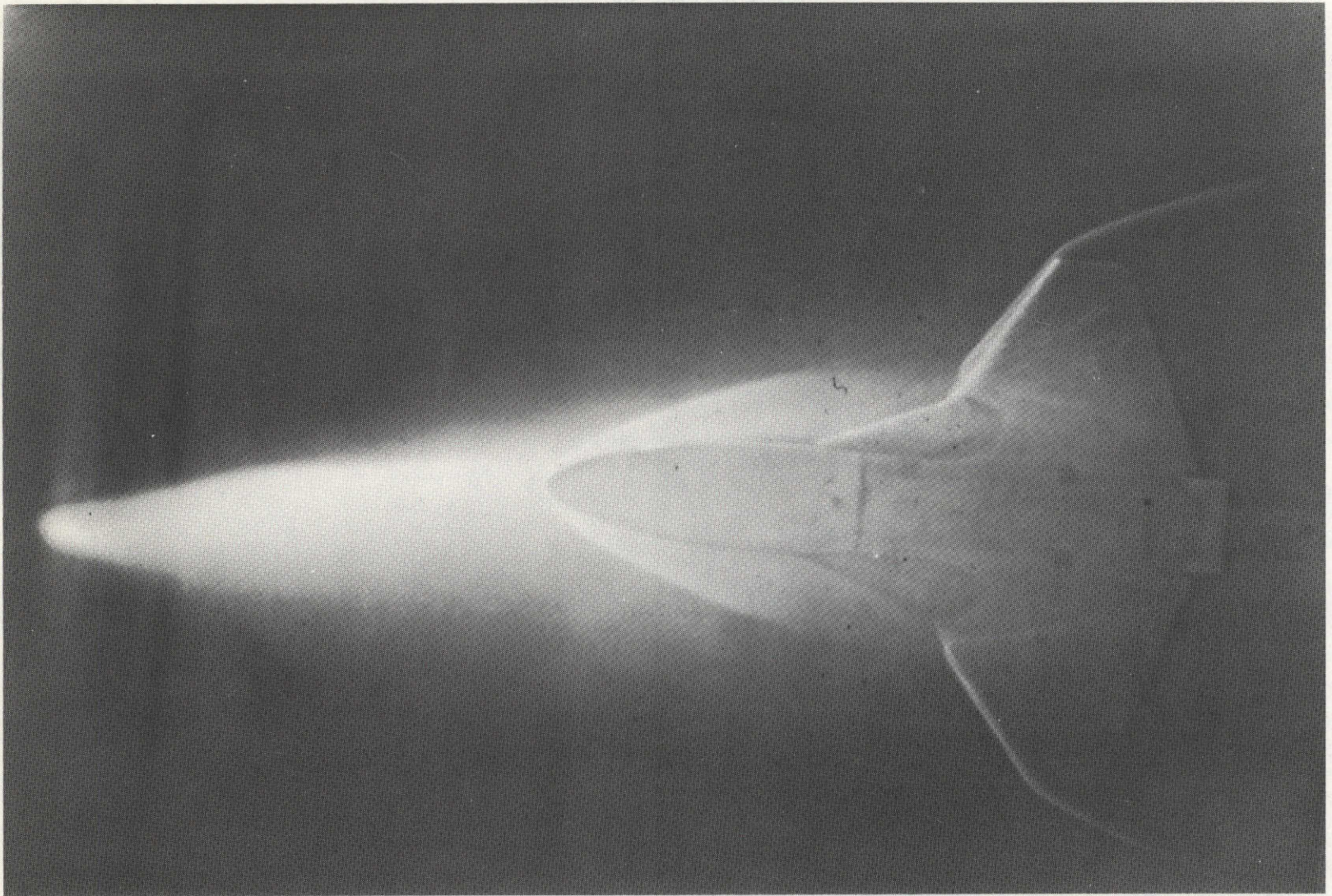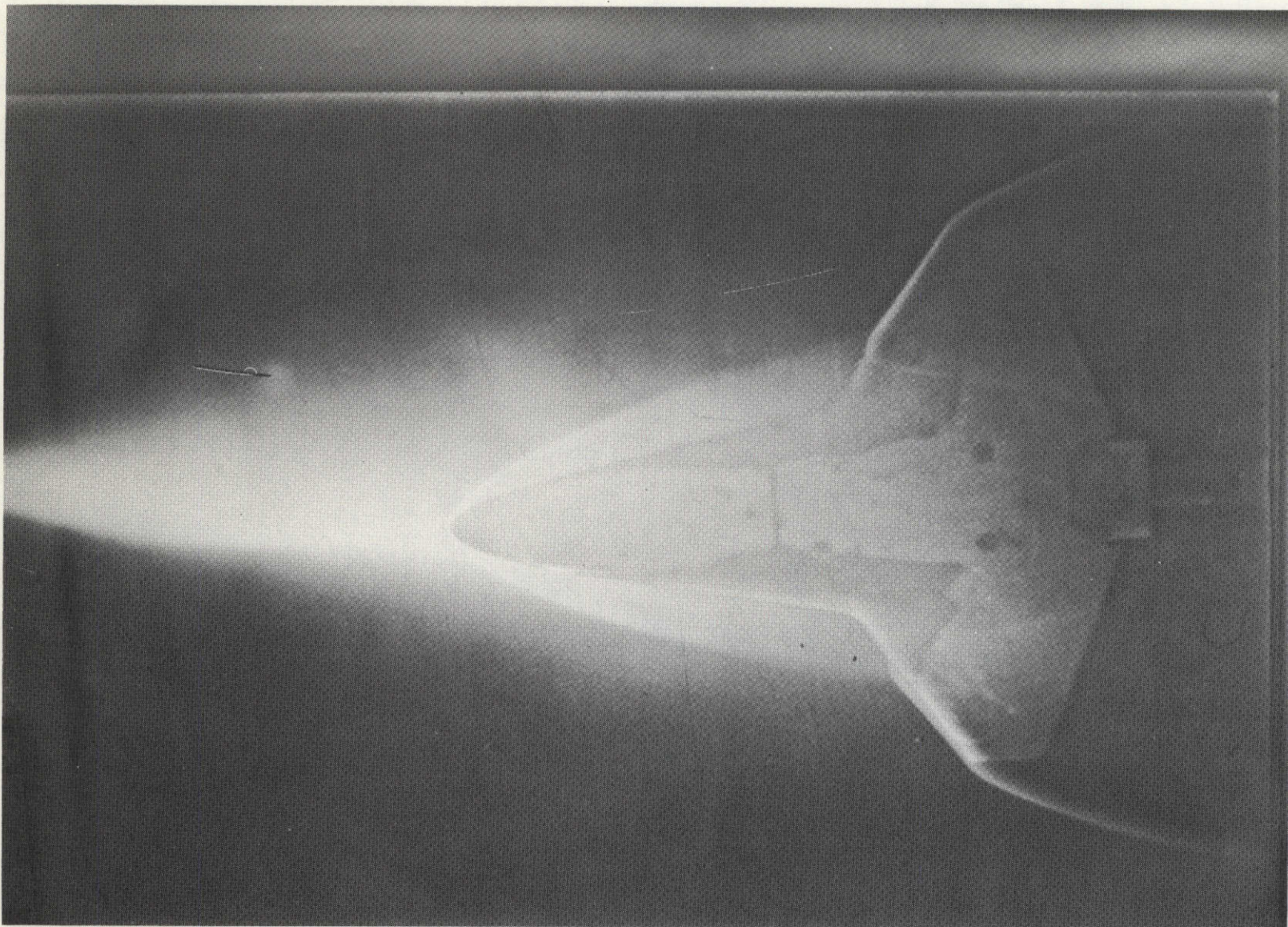
Figure 21.- Concluded.

(a) Basic wing.

L-74-1107

Figure 22.- Electron beam using wing 3. $\alpha = 30^O$.

(b) 70° fillet.

L-74-1108

Figure 22.- Continued.

(c) 78° fillet.

Figure 22.- Concluded.